Development of Programmable Front-End Electronics for Use with Ultrasound Hydrophone

A Thesis

Submitted to the Faculty

of

Drexel University

by

Sumet Umchid

in partial fulfillment of the

requirements for the degree

of

Master of Science in Biomedical Engineering

August 2003

ACKNOWLEDGMENTS

I would like to acknowledge the following people for their contributions to the completion of this thesis; I would like to whole-heartedly thank my advisor, Dr. Peter A. Lewin for his guidance. The accomplishment of this study would not have been possible without his advice and encouragement.

Next, I thank my co-advisor, Dr. Philip E. Bloomfield, for his support and direction. His contribution has made all of this possible and has enhanced the quality of the work.

Also, I would like to thank Dr. Ryszard Lec for serving on my committee and Dr. Emil G. Radulescu for all his advice and support.

More importantly, I would like to thank my parents, sister and brother for giving me unconditional love and support from the other side of the world.

TABLE OF CONTENTS

LIST OF TABLES

LIST OF FIGURES

ABSTRACT

Development of Programmable Front-End Electronics for use with ultrasound hydrophone

Sumet Umchid

Peter A. Lewin, Ph.D.

Philip E. Bloomfield, Ph.D.

Piezoelectric sensors are widely used in many bioengineering applications. However, the sensors exhibit high, on the order of MegaOhms, output impedance and, therefore, the signal generated at the output terminals of a sensor needs to be electronically conditioned prior to further use. Specifically, it is necessary to incorporate a high quality preamplifier between the sensor and analyzing equipment. Such preamplifiers are not commercially available. This work describes development of a programmable preamplifier tailored for use with miniature piezoelectric polymer hydrophones for characterization of acoustic output of ultrasound scanners. Such scanners are used in almost all medical fields and are becoming the preferred imaging modality in a variety of clinical situations. The preamplifier features 50Ω output impedance to eliminate transmission line phenomena, and high input resistance (1MΩ) which minimizes loading of the hydrophone. The frequency response of the preamplifier was optimized to comply with the Food and Drug Administration (FDA) requirements; the circuit operates between 100 kHz and 40 MHz. To optimize the performance in terms of input impedance, frequency response and dynamic range, the preamplifier was implemented in two stages using application specific operational amplifiers. Visual Basic program was employed to automatically execute On/Off function of the buffer circuit. The implemented circuit topology allows fully automatic determination of key acoustic output parameters of diagnostic ultrasound

scanners, which, in turn, determine the safety indicators such as Mechanical Index (MI) and Thermal Index (TI).

To verify the performance of the programmable preamplifier, several ultrasound hydrophones were measured and calibrated with and without preamplifier. The measurement results are presented in terms of end-of-cable voltage sensitivity as a function of frequency. Also, the impedance of the preamplifier and programmable buffer circuit were determined as a function of frequency. In addition, the circuit's scattering parameter S_{21} that is its transfer function versus frequency was measured. Future work will focus on extension of the preamplifier's bandwidth up to 100 MHz.

CHAPTER 1.0: INTRODUCTION

In the past few decades, medical diagnostic ultrasound has become the primary non-invasive imaging modality because it does not emit ionizing radiation such as X-ray and also provides real-time information of the anatomical structures. However, under certain conditions ultrasound exposure in general may introduce biological effects [1]. Therefore, the output acoustic pressure of the diagnostic ultrasound devices is regulated and cannot exceed prescribed limits. In the USA, these prescribed limits are established by the Food and Drug Administration, Center for Devices and Radiological Health, which requires the safety indicators such as Mechanical Index (MI) and Thermal Index (TI) to be displayed on the ultrasound imaging systems. Determination of these two indices requires precise measurement of the acoustic pressure-time waveforms produced by the imaging transducer.

In order to obtain the faithfully reproduced acoustic pressure-time waveforms, it is desirable to incorporate a high quality voltage preamplifier between the piezoelectric sensor or hydrophone and the associated analyzing equipment. This is because the output voltage signal generated by the hydrophone is developed across an extremely high, on the order of hundred kOhms, electrical impedance. Therefore, a preamplifier is needed to convert the high output impedance of the hydrophone to a lower value that is much less susceptible to loading by the relatively low input impedance of the measuring instrument used to display or record the acoustic pressure-time waveforms.

The purpose of this work was to design, simulate, prototype and test a preamplifier and a programmable buffer circuit with ultrasound hydrophones in the frequency range of 100 kHz to 40 MHz in order to match an output impedance of the hydrophone to an input impedance of the analyzing equipment, and optimize the sensitivity and frequency response of ultrasound hydrophone. The significance of this research and the scope of the work are presented in the subsequent sections.

1.1 Motivation

As already mentioned the output voltage signal generated by a piezoelectric active element in the hydrophone is developed across an extremely high impedance and is of very low power content, which causes the loading effects. Therefore, in order to eliminate loading effects and signal distortion, it is essential that the signal from a hydrophone is routed through a preamplifier before applying it to measuring and recording instrumentation [2, 3].

Consequently, when properly designed, the preamplifier is a useful device in an acoustic measurement chain. It can increase the overall hydrophone's sensitivity, which is beneficial in cases where the measured pressure amplitude is relatively low or when a significant finite amplitude distortion in the pressure wave is present [2, 3]. Moreover, the preamplifier increases the frequency response at the low frequency of the system by decreasing the low cut-off frequency and also eliminates the reflection effect from the

transmission line phenomena. However, some trade-off to using a preamplifier is that it adds to the complexity and the cost of the hydrophone [4].

Although the acoustic measurement system used is almost fully controlled automatically by a computer program, the measurements take a long time due to careful alignment and calibration procedures (for certain hydrophones it may take more than 8 hours). However, the acoustic source, such as a very wideband transducer, is a sensitive device that should not be overexcited for a prolonged period of time. Therefore, the programmable buffer circuit is needed to automatically control On/Off function of the signal exciting the acoustic source. With the application of the programmable buffer circuit, whenever the calibration process is done, the signals exciting the acoustic source are automatically cut off.

For medical diagnostic ultrasound devices, their -3 dB frequency bandwidth normally begins in the low megahertz range and can extend beyond the 40 MHz range [5]. The optimization of harmonic imaging techniques will require field parameters to be measured above 15-20 MHz. However, many new clinical applications of ultrasound imaging at frequencies greater than 15-20 MHz have been under development for some years. The use of these frequencies enables the transcutaneous exploration of superficial tissues in fields such as dermatology, ophthalmology and microsurgery [6]. Presently the field of high ultrasonic frequency ranges from 15-20 to 150-200 MHz, providing a very high spatial and temporal resolution. However, the increased signal losses in tissue

(attenuation) associated with higher ultrasound frequencies naturally limits imaging depth [6].

High ultrasonic frequencies (10-30 MHz) were first used to measure skin thickness [7, 8]. Frequencies between 15 and 50 MHz were tested in B-mode imaging with encouraging results, but no efficient systems were used routinely, generally due to poor probe performance [9, 10]. Indeed the probes often had a too narrow fractional bandwidth and provided poor axial resolution. Before the new piezoelectric materials such as polymers (PVDF, poly(vinylidene fluoride)) and small grain size (3-6 μm), high density piezoceramics (PZT) were discovered, Foster's Canadian team built small focused ultrasonic transducers in the 40–100 MHz frequency range [11, 12]. With these high performance transducers and associated electronic devices they obtained remarkably good images of cutaneous tissues, the anterior chamber of the eye and mouse embryos [11, 13, 14]. The high frequencies were also suitable to detect and measure blood flow in microcirculation. Frequencies around 100 MHz were proposed first [15, 16]. Then Foster's team presented a duplex system with a duplex probe comprising a 60 MHz imaging transducer and a 40 MHz continuous wave Doppler transducer [17]. The same team recently built a high frequency pulsed wave Doppler system using a 50 MHz PVDF transducer [18], which can detect and measure blood velocities of less than 5 mm/s in arterioles and venules with diameters as small as 20 and 30 μm, respectively.

However, the frequency range below 1 MHz is also important in the field of ultrasound metrology. Information about these lower frequencies is used to determine the

Mechanical Index (MI). The MI is widely accepted as one of the critical safety indicators for diagnostic ultrasound. It provides a numerical indication of the potential for mechanical damage to insonified tissue and is required to be displayed in real-time on the screen of modern ultrasound imaging devices [19]. It has been shown that minimization of the overall uncertainty in the MI determination to about 5% requires the hydrophone bandwidth on the order of one twentieth of the fundamental imaging frequency [20]. With the introduction of harmonic imaging, scanheads operate at center acoustic frequencies down to 2 MHz; therefore there is a need for ultrasonic hydrophone probes calibrated down to 100 kHz [21].

Accordingly, this work was centered on design and development of a programmable preamplifier in the frequency range between 100 kHz and 40 MHz. The performance of the preamplifier has been tailored for use with miniature piezoelectric polymer hydrophones for characterization of acoustic output of ultrasound scanners. The preamplifier features high input impedance (1MΩ) which minimizes loading of the hydrophone, and 50Ω output impedance to eliminate transmission line phenomena. The scope of the work and the programmable preamplifier's design criteria are discussed below.

1.2 Scope of the Work

This work is divided into four major sections. Chapter 2.0 gives a brief background on the entire work, which is composed of two main parts: Electronic and Acoustic Part. For section 2.1, the key electronic parameters of the programmable preamplifier circuits are overviewed whereas section 2.2 summarizes the acoustic filed parameters needed for optimization of the electronics. Section 2.1.3 discusses electronic transfer function in terms of S_{21} scattering parameter. Additionally, the acoustics part in section 2.2 describes the state-of-the art in preamplifiers, different hydrophone probes and their properties, and hydrophone calibration using Time Delay Spectrometry (TDS).

The methodology with a roadmap of the work is described in chapter 3.0. Section 3.1 discusses design constrains and gives a general description of the preamplifier and the programmable buffer circuit. Sections 3.1.1 and 3.1.2 detail necessary conditions to obtain a high performance circuit topology of the programmable preamplifier such as slew rate effect, power supply limitation, bypass capacitance, and feedback resistance values. The Pspice simulation, carried out to verify the circuit topologies presented in sections 3.1.1 and 3.1.2, is examined in section 3.2.

The fabrication of prototypes of preamplifier and programmable buffer required careful attention to their boards' layout in order to achieve optimum performance at high frequencies and to minimize the influence of parasitic and stray capacitances. These details are included in section 3.3. Section 3.4 describes the experimental tests. The

electronic test described in section 3.4.1 used advance network analyzer techniques for determining the preamplifier's and programmable buffer circuit's key characteristics. The impedance measurements are described in section 3.4.1.1 whereas transfer function measurements, in terms of S_{21} Scattering parameter, are given in section 3.4.1.2. Section 3.4.2 details the acoustic test measurement set-up.

Results from the simulations, prototyping and experimental tests are summarized in chapter 4.0. Section 4.1 shows results of Pspice simulations of the designed circuit topologies and section 4.2 presents a picture of the preamplifier and programmable buffer circuit's prototypes. The impedance and transfer function (S_{21}) of the programmable preamplifier, and the end-of-cable voltage sensitivity versus frequency of a hydrophone probe tested with the programmable preamplifier assembly are given in section 4.3. These results were carried out in the frequency range of 100 kHz - 40 MHz at discrete intervals (200 kHz).

Discussion and conclusions of the work are presented in chapter 5.0, and the suggestions for future work are given in chapter 6.0.

Several appendices are included to further elucidate the approach of the work. Appendix A lists the symbols used throughout the works. Appendix B provides Visual Basic code developed to control programmable buffer circuit On/Off. Finally, Appendix C details the board layout guidelines.

CHAPTER 2.0: BACKGROUND

This chapter provides the background information that summarizes the fundamentals of operational amplifiers and briefly outlines experimental methods used to evaluate their performance. Also, ultrasound hydrophone designs and their electrical equivalent circuits are presented. This information was used in designing the wideband preamplifier and programmable buffer circuit assembly described later.

2.1 Electronic Part

2.1.1 Basic Operational Amplifiers

One of the most useful and widely used devices in electronic instrumentation is the Operational Amplifier (OP-AMP) shown diagrammatically in Figure 2.1. It has gradually evolved from the large vacuum tube devices, to those using discrete transistor, and now to the small integrated circuit devices [22]. OP-AMPs can amplify DC as well as AC signals.

An ideal OP-AMP has infinite input impedance, infinite voltage gain, zero output impedance, and infinite bandwidth [23]. Also, it can be connected as a perfect differential amplifier. A differential amplifier has two inputs, and ideally responds only to the difference between signals applied to these two inputs.

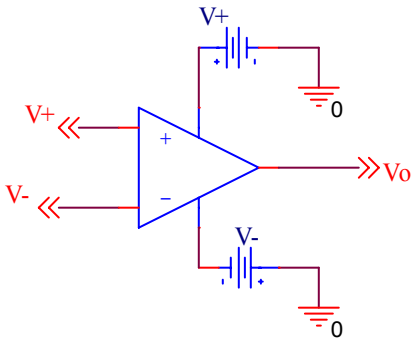

Figure 2.1: The symbol for an OP-AMP with two inputs; the inverting input (-) and the non-inverting input (+).

The output signal (voltage) in Figure 2.1, V_o, is given by:

$$V_o = A(V_+ - V_-) \tag{2.1}$$

where V_+ and V_- are the signals applied to the non-inverting and to the inverting input, respectively. A represents the open loop gain of the OP-AMP. A is infinite for the ideal amplifier, whereas for the various types of real OP-AMPs, it is usually within the range of 10^4 to 10^6.

OP-AMPs can be thought of as a gain block, a component whose function is to amplify. Biasing does not represent any serious challenge because all the necessary components are built into the chip. Amplifier design is also relatively simple; the OP-AMP gain is so high that practical performance depends only on external components [22].

Since the open loop gain of OP-AMPs is very high, OP-AMPs are almost exclusively used with some additional circuitry (mostly with resistors and capacitors), required to ensure a negative feedback loop. Through this loop a tiny fraction of the output signal is fed back to the inverting input. The negative feedback stabilizes the output within the operational range and provides a much smaller but precisely controlled gain, the so-called closed loop gain. The typical applications of OP-AMPs are briefly described in the next section.

2.1.2 Applications of Operational Amplifiers

OP-AMPs can be used to perform many tasks. They can be used to amplify and invert a signal, amplify a signal, buffer a signal, add two different signals, subtract two different signals, integrate a given signal, or differentiate a given signal. The following section explains the application of OP-AMPs:

2.1.2.1 Inverting Amplifier

The basic circuit of the inverting amplifier is shown in Figure 2.2.

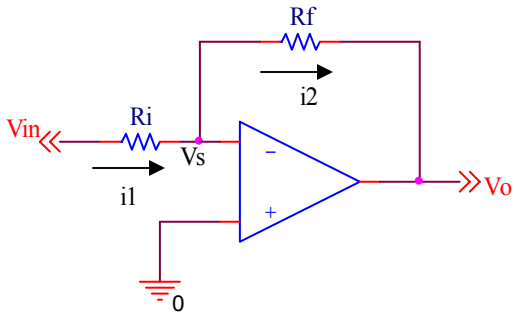

Figure 2.2: Inverting Amplifier.

The transfer function is derived as follows: Considering the arbitrary current directions:

$$i_1 = (V_{in} - V_s)/R_i \tag{2.2}$$

and

$$i_2 = (V_s - V_o)/R_f \tag{2.3}$$

The non-inverting input is connected directly to the circuit common (i.e. $V_+ = 0$ V), therefore $V_s = V_- = 0$ V:

$$i_1 = V_{in}/R_i \tag{2.4}$$

and

$$i_2 = -V_o/R_f \tag{2.5}$$

Since there is no current flow to any input (ideal OP-AMP exhibits infinitely high input resistance); $i_1 = i_2$

Therefore, the transfer function of the inverting amplifier is

$$V_o = -(R_f / R_i)V_{in} \tag{2.6}$$

Thus, the closed loop gain of the inverting amplifier is equal to the ratio of R_f (feedback resistor) over R_i (input resistor). This transfer function describes accurately the output signal as long as the closed loop gain is much smaller than the open loop gain A of the OP-AMP used (e.g. it must not exceed 1000), and the expected values of V_o are within the operational range of the OP-AMP [22].

2.1.2.2 Summing Amplifier

The summing amplifier is a logical extension of the Inverting Amplifier circuit, with two or more inputs. Its circuit is shown in Figure 2.3.

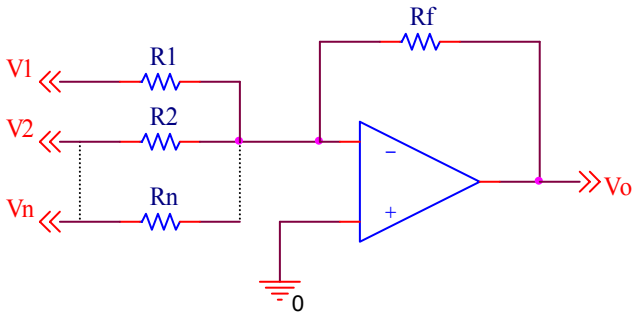

Figure 2.3: Summing Amplifier.

The transfer function of the summing amplifier (similarly derived) is:

$$V_o = -(V_1 / R_1 + V_2 / R_2 + ... + V_n / R_n)R_f \tag{2.7}$$

Thus if all input resistors are equal, the output is a scaled sum of all inputs, whereas, if they are different, the output is a weighted linear sum of all inputs.

The summing amplifier is used for combining several signals. The most common use of a summing amplifier with two inputs is the amplification of a signal combined with a subtraction of a constant amount from it (dc offset).

2.1.2.3 Difference Amplifier

Difference amplifier precisely amplifies the difference of two input signals. Its circuit implementation is shown in Figure 2.4.

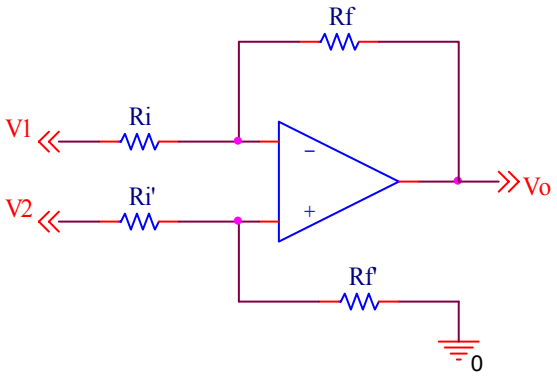

Figure 2.4: Difference Amplifier.

If $R_i = R_i'$ and $R_f = R_f'$, then the transfer function of the difference amplifier is:

$$V_o = (V_2 - V_1)R_f / R_i \tag{2.8}$$

The difference amplifier is useful for handling signals referring not to the circuit common, but to other signals, known as floating signal sources [22]. Its capability to reject a common signal makes it particularly valuable for amplifying small voltage differences contaminated with the same amount of noise (common signal).

In order for the difference amplifier to be able to reject a large common signal and to generate at the same time an output precisely proportional to the two signals difference, the two ratios $p = R_f/R_i$ and $q = R_f'/R_i'$ must be precisely equal, otherwise the signal output will be:

$$V_o = [q(p+1)/(q+1)]V_2 - pV_1 \tag{2.9}$$

2.1.2.4 Instrumentation Amplifier

Instrumentation Amplifiers (IA) are used when it is necessary to measure low-level differential signals with a high degree of accuracy. The difference amplifier is not entirely satisfactory as an instrumentation amplifier because its major drawbacks are its low input impedance and its gain cannot be easily varied [23]. An instrumentation amplifier circuit is shown in Figure 2.5

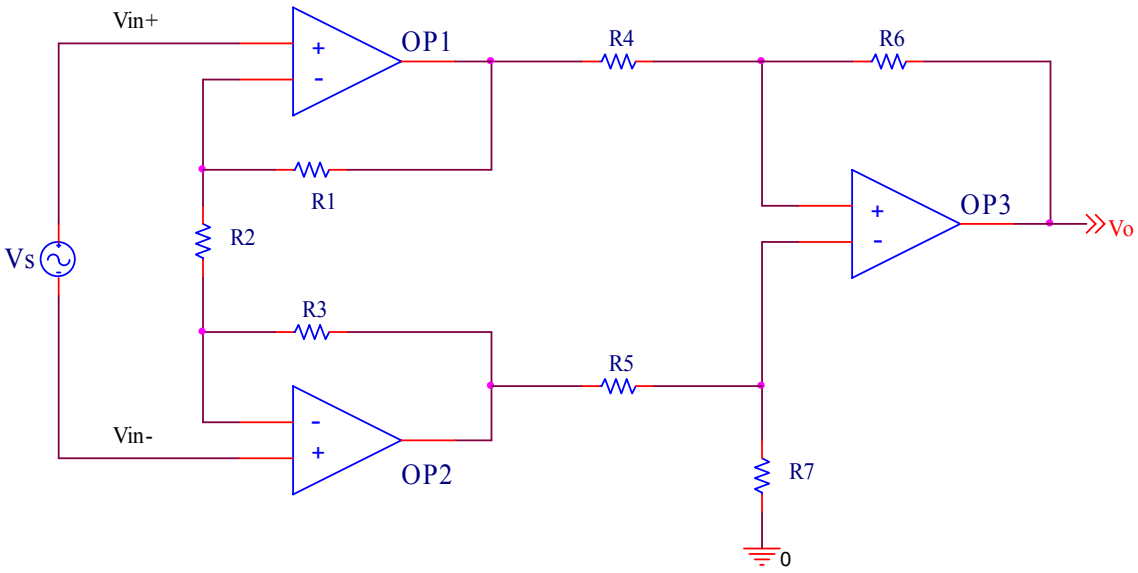

Figure 2.5: Instrumentation Amplifier.

The circuit consists of two stages: The first stage is a buffered amplifier, which is formed by OP-AMPs OP1 and OP2, and their associated resistors. The second stage is formed by a basic differential amplifier OP3 together with its four associated resistors.

The instrumentation amplifier offers two useful functions: it amplifies the difference between inputs and rejects the signal that's common to the inputs. The latter is called Common Mode Rejection (CMR). The signal gain is provided by OP1 and OP2 while OP3 typically forms a differential gain of 1. The overall gain of the instrumentation amplifier can be calculated as:

$$\frac{V_o}{V_s} = \left(1 + 2\frac{R_1}{R_2}\right)\frac{R_6}{R_4} \tag{2.10}$$

where R_1=R_3 and $R_5/R_4 = R_6/R_7$.

From equation 2.10, it can be seen that the gain can be adjusted by varying the single resistor R_2.

Since both the input-stage op amps are connected in the noninverting configuration, the input impedance seen by Vin- and Vin+ is (ideally) infinite, which is a major advantage of the instrumentation amplifier configuration [22].

2.1.3 Scattering Parameters (S-parameters)

A scattering matrix (S-parameter matrix) is one way to describe the operation of a linear, time-invariant two-port circuit. A two-port network is defined as any linear device where a signal goes in one side and comes out the other [24].

The measurement setup associated with S-parameters is shown in Figure 2.6.

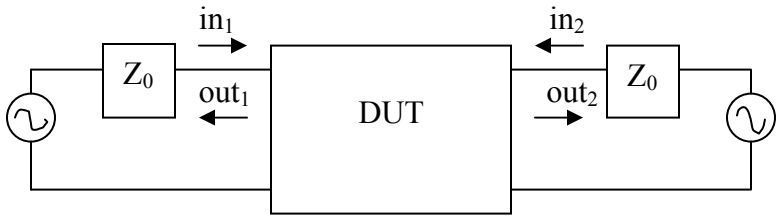

Figure 2.6: A two-port S-parameter matrix records the reflection coefficients and transmission gain for signals coming and going on both sides of the device under test (DUT).

From the test equipment, two cables having characteristic impedance Z_0 lead to the left and right sides, respectively, of the device under test (DUT).

Using the first (left-hand side) cable, a sinusoidal signal (in_1) of unit amplitude is injected into the DUT. The test equipment records the amplitude and phase of the signal (out_1) reflected back into the first cable from the DUT, and also the amplitude and phase of the signal (out_2) conveyed through the DUT to the second cable on the other side.

Using the second (right-hand side) cable, another sinusoidal signal (in_2) of unit amplitude is injected into the DUT. The test equipment records the amplitude and phase of the signal (out_2) reflected from the right hand side of the DUT, and the amplitude and phase of the signal (out_1) conveyed through the DUT to the other (left) side. The complete S-parameter matrix is a combination of these four basic measurements.

The left column of the S-parameter matrix is defined when injecting a signal from the left:

$$S_{11} = \frac{out_1}{in_1} \text{ (L-side reflection)} \tag{2.11}$$

and

$$S_{21} = \frac{out_2}{in_1} \text{ (L} \rightarrow \text{R transmission)} \tag{2.12}$$

The right column of the matrix is defined when injecting a signal from the right:

$$S_{12} = \frac{out_1}{in_2} \text{ (R} \rightarrow \text{L transmission)} \tag{2.13}$$

and

$$S_{22} = \frac{out_2}{in_2} \text{ (R-side reflection)} \tag{2.14}$$

The four elements of the s-parameter matrix then may be used to compute the signals out_1 and out_2 deriving from the two-port device when stimulated by input signals in_1 and in_2:

$$out_1 = S_{11} * in_1 + S_{12} * in_2 \tag{2.15}$$

and

$$out_2 = S_{21} * in_2 + S_{22} * in_2 \tag{2.16}$$

The four elements of an S-parameter matrix may be reported as complex numbers (with real and imaginary parts) or in logarithmic units (as magnitude in dB and phase in radians).

The procedure above provides a model for the calculation of circuit performance only at one single frequency. Therefore, the entire measurement procedure is usually performed on a dense grid of frequencies spanning the range of interest [24].

2.2 Acoustic Part

2.2.1 Preamplifiers

As already noted the acoustic field including its spatial distribution is characterized using piezoelectric hydrophones. The hydrophone's (circular) active element is usually on the order of 0.5 mm and therefore its capacitance is relatively low.

Loading of a hydrophone's output even by relatively high impedance loads, can greatly reduce its sensitivity (in μV/Pa or dB re 1μV/Pa) as well as severely limit its frequency response. To prevent or help minimize these effects it is essential that the signal from a hydrophone is fed through a preamplifier before applying it to measuring and recording instrumentation [2, 3].

Normally, a preamplifier serves two basic functions. First is to convert the high output impedance of the hydrophone to a lower value that is much less susceptible to loading by the relatively low input impedance of the measuring instrument used. Second is to amplify the relatively weak output signal from the hydrophone so as to obtain sufficient signal power to drive the measuring instrumentation. The first reason is perhaps the most important. Providing that the preamplifier has sufficiently high input impedance and does not load the output of the hydrophone, it will produce an output voltage proportional to the input voltage. Such operating preamplifier is referred to as voltage amplifier. Although design of charge amplifier is possible in this work, only voltage preamplifier design was considered.

The voltage preamplifier is based on the use of a hydrophone as a voltage source. This requires that the preamplifier input impedance is very high in order to avoid loading which can influence the voltage sensitivity vs. frequency characteristics of the hydrophone. In practice, loading is unavoidable as even with voltage preamplifiers that have the highest possible input impedance the parallel capacitance of the hydrophone output connection cable (C_c) has to be considered [4]. The reasons for this can be explained with reference to the simplified voltage preamplifier equivalent circuit shown in Figure 2.7.

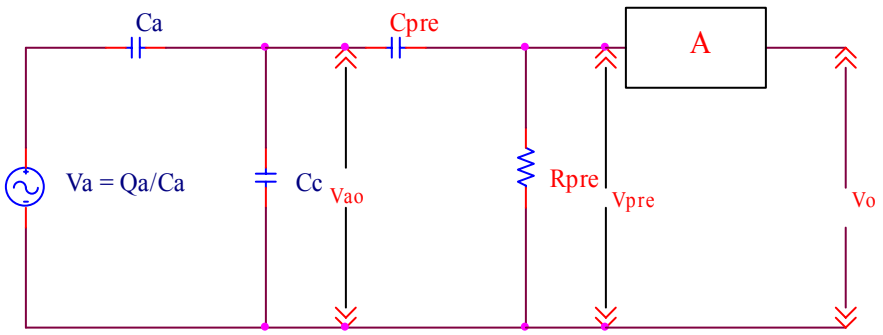

Figure 2.7: Equivalent circuit of voltage preamplifier using a hydrophone as a voltage source.

Also, from Figure 2.7, it can be seen that the charge Q_a produced by a hydrophone when exposed to acoustic pressure appears as a voltage V_a. This voltage is developed across the internal capacitance C_a of the hydrophone and the parallel capacitance C_c of the output connection cable. Together C_a and C_c act as a frequency independent voltage divider network which attenuates V_a to produce the output voltage V_{ao}. Thus a hydrophone's voltage sensitivity S_v depends not only on its charge sensitivity S_q and capacitance C_a, but also on the parallel capacitance C_c of its output connection cable. This is shown by the relation:

$$S_v = \frac{S_q}{C_a + C_c} \tag{2.17}$$

Unlike S_q and C_a which are hydrophone constants, C_c is dependent on cable length. Therefore, with long connection cables the voltage sensitivity of a hydrophone will be significantly reduced as the attenuation due to C_a and C_c will be high. Also, if the length of the cable is changed, the attenuation will be altered meaning that new voltage

sensitivity for the hydrophone has to be determined. The use of voltage preamplifier is therefore only recommended with fixed, relatively short lengths of cable connecting the hydrophone and preamplifier. However, an ultrasonic hydrophone probe with a built-in preamplifier is one way to optimize the sensitivity of the hydrophone and minimize the length of cable effects. A detailed description of integrated preamplifier for ultrasound hydrophone probe can be found in [4].

The input impedance of voltage preamplifiers influences the voltage sensitivity characteristics of hydrophone primarily at low frequencies. At these frequencies the combined reactance of C_a and C_c with C_{pre} the AC input coupling capacitance of the preamplifier, starts to become appreciable compared with the input resistance R_{pre} of the preamplifier. Together these components form a frequency dependent voltage divider network which attenuates the hydrophone voltage V_{ao} and the preamplifier input voltage V_{pre}, thus determining the low frequency roll-off of the hydrophone and preamplifier. The frequency at which $V_{pre} = 0.707V_{ao}$ is termed the -3dB lower limiting frequency which is given by:

$$f_L = \frac{C_a + C_c + C_{pre}}{2\pi R_{pre}(C_a + C_c)C_{pre}} \tag{2.18}$$

With direct coupled voltage preamplifier a lower -3dB lower limiting frequency is obtained as an input coupling capacitor C_{pre} can be omitted and equation 2.18 can be expressed as:

$$f_L = \frac{1}{2\pi R_{pre}(C_a + C_c)} \tag{2.19}$$

2.2.2 Hydrophones

Hydrophones are the universal instruments used to characterize the acoustic output of medical diagnostic ultrasound devices. Hydrophones generate an electrical output when subjected to acoustic pressure. Over a wide dynamic range and frequency range, their voltage output is directly proportional to the acceleration of the acoustic pressure. The performance of hydrophones is related to their physical characteristics; therefore many designs have emerged that vary in dimensions and in the piezoelectric material used as the sensitive element. The materials that have been used for ultrasonic hydrophones include solid piezoelectric ceramics (i.e. lead zirconate titanate, PZT), single crystals (i.e. quartz or tourmaline), and polymers (i.e. polyvinylidene fluoride, PVDF). Ceramic and crystal-based hydrophones have a tendency not to meet the important criteria necessary for high performance hydrophones such as wide bandwidth, high dynamic range, and smooth, wide-angle directivity. They also suffer from radial resonances and a non-uniform frequency response. For these reasons, most commercial ultrasonic hydrophone probes are constructed with PVDF as the sensitive element [25]. Accordingly, all design considerations presented in this work assumed that the input voltage to the preamplifier is generated by PVDF made probes.

There are two basic PVDF hydrophone designs [25-29]: the spot-poled membrane and the Lewin or needle-type hydrophone [25]. Both types exhibit active element on the order

of or less than 0.5 mm. The sensitive element thickness is typically in the range of 9 to 50 μm and, to a large extent, controls the bandwidth of the probe. Details in the design and fabrication of these hydrophones are explored in the next two sections.

2.2.2.1 Membrane hydrophone

The spot-poled membrane hydrophones, which are typically more popular and somewhat more durable than the tapered needle style are a laminated structure comprising two layers of 15 μm PVDF; this PVDF is stretched over a supporting hoop as shown in Figure 2.8. The size of the hoop is around 100 mm in diameter, to allow the acoustic beam from an acoustic source to pass through its aperture [28]. The small region in the center (0.5-1 mm in diameter) [27], known as the active element, is poled and electroded.

The membrane hydrophone has been found to be acoustically transparent from 1 to 15 MHz. This hydrophone resonates in the fundamental thickness mode at 1/2 ultrasonic wavelength (λ/2). For the 30 μm total thickness of the PVDF membrane the resonance occurs at ~37 MHz. Radial resonance modes occur well below the frequency of interest and are highly damped as a result of a large diameter membrane with no backing [28]. Normally, the frequency response is flat below the resonance and decays beyond the resonance. However, the membrane features non-uniform angular response in the low megahertz range when sound is incident at the critical angle ($\approx 50°$) [25, 27]. Standing waves can also be evident in acoustic measurements of transducers generating continuous wave signals [28].

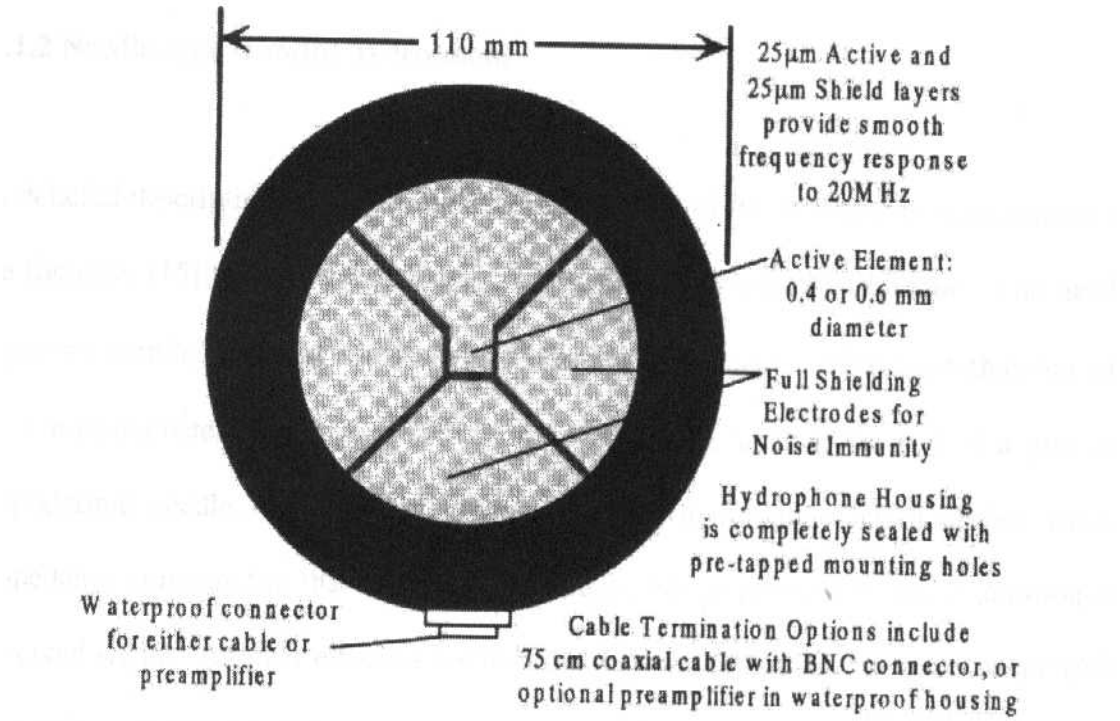

Figure 2.8: Schematic of a typical PVDF membrane hydrophone (Courtesy of Perceptron, Hatboro. PA 19040), now Sonore Medical Systems, Inc, Longmont, CO.

In the past several years, the development has been made in extending the -3 dB bandwidth of ultrasonic hydrophone probes. Lum et al [30] created a membrane hydrophone from a 4 μm thick film of vinylidene fluoride trifluoroethylene copolymer, P(VDF-TrFE). Preliminary measurement results have shown that the VDF co-polymer hydrophone had an effective spot diameter of less than 100 μm and a -3 dB bandwidth that extended to 150 MHz. While further work must be done to fully characterize the frequency response above 20 MHz and to accurately measure the effective diameter of the sensitive area, this membrane hydrophone showed potential to faithfully determine the frequency and spatial parameters of ultrasonic diagnostic transducers in the 10-40 MHz range [30].

2.2.2.2 Needle-type (Lewin) hydrophone

The Needle-type hydrophones have a coaxial construction of stainless steel and various insulating materials. The active end is tapered, with a flat tip ground to the nominal diameter in microns. Figure 2.9 shows a schematic of a needle-type hydrophone. This type of hydrophone consists typically of a 25 μm thick circular PVDF film, with either a 0.6 or seldom 1 mm diameter. The backing material of the hydrophone has a higher acoustic impedance compared to that of water (1.5 MRayl), that makes it one-quarter wavelength thickness (λ/4) resonance frequency. A detailed description of the design and construction of the needle-type hydrophone can be found in [29].

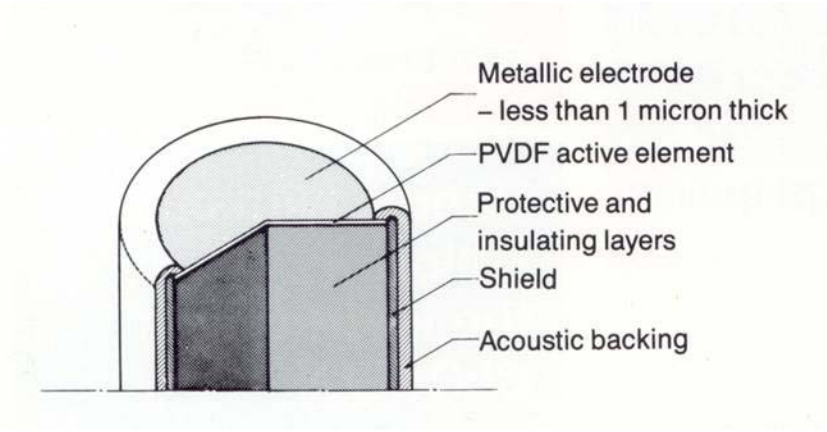

Figure 2.9: Schematic diagram of a needle hydrophone (Courtesy of Force Institutes, Copenhagen, Denmark).

2.2.3 Hydrophone Properties

2.2.3.1 Linearity

Linearity is an important parameter in the characterization of ultrasonic hydrophone. For the testing of medical diagnostic and therapeutic equipment, the hydrophone should exhibit linearity to at least the relevant acoustic pressure output from these devices. The ultrasonic diagnostic imaging equipment can generate instantaneous pressure amplitudes on the order of 10 MPa [25]. Therefore, the hydrophone sensitivity must be linear over that range.

Meeks and Ting [31] provided evidence that PVDF polymer is linear to about 65 MPa. They acquired the linearity response as a function of dynamic pressure pulses with a rise time of 1-3 ms and peak amplitudes up to 75 MPa. The deviations of linearity at 65 MPa for the different types of PVDF polymers tested were less than 7% when compared to ideal linearity response [31].

2.2.3.2 Frequency response

Theoretically, a hydrophone should convert the acoustic pressure waveform into a corresponding voltage waveform. Frequency response of hydrophones is the hydrophone sensitivity as a function of frequency. The frequency response of the hydrophone and associated electronics should be flat over the whole range of frequencies, which are

contained in the waveform in order to reproduce the pressure-time waveform correctly. Smith [32] has shown that the thickness of the active hydrophone element and the cable length can also influence the frequency response. A relatively thick element gives rise to a lower resonance frequency, which reduces the -3 dB frequency bandwidth of the hydrophone. For example, compared to a 50 μm thick membrane, a 9 μm thick membrane hydrophone has a flat frequency response over a frequency range approximately 5 times greater. The results of Smith's work suggest that the cable resonance has a greater impact on the frequency response than the thickness-mode resonance and suggests minimizing cable length to about 15 cm [32].

Incorporating a preamplifier into the hydrophone assembly has also been shown to overcome the loading effects introduced by the cable [4]. The preamplifier will also increase the hydrophone sensitivity, which is beneficial in cases where the measured pressure amplitude is very low or when a significant finite amplitude distortion in the pressure wave is present [2, 32]. Some trade-off to using a preamplifier is that it would add to the complexity and the cost of the hydrophone and it could limit the dynamic range [4]. Also, the bandwidth of the preamplifier must be considered in order to minimize the errors introduced by non-ideal frequency responses [33]. Moreover, accessory electronic components could have an impact on hydrophones performance. Good radio frequency (RF) shielding is required to reduce the noisy environment created by the medical ultrasonic equipment.

2.2.3.3 Hydrophone sensitivity

One of the goals in the ultrasound metrology is to determine the voltage sensitivity by measuring the voltage at the hydrophone terminals. The end-of-cable loaded sensitivity of a hydrophone, $M_L(f)$, is calculated from equation 2.20**,** when used in a continuous single-frequency sound field of frequency *f*:

$$M_L(f) = \frac{v}{p} \tag{2.20}$$

where v is the voltage generated by the acoustic pressure incident on the sensitive element of the hydrophone and p represents the free-field acoustic pressure at the hydrophone. $M_L(f)$ should be expressed as a function of f when it is important to emphasize that the hydrophone sensitivity may vary with frequency.

The end-of-cable open-circuit sensitivity $M_c(f)$, is a convenient way to specify sensitivity independent of the loading conditions; however, it is difficult to measure since it assumes that at the time of calibration, the measured hydrophone voltage was loaded with an infinite resistance (open-circuit) [4]. Once the end-of-cable loaded sensitivity has been measured, the open-circuit sensitivity can simply be calculated using the following relationship [25]:

$$M_L = M_C \sqrt{\frac{\{\mathrm{Re}(Z_{el})\}^2 + \{\mathrm{Im}(Z_{el})\}^2}{\{\mathrm{Re}(Z_{el}) + \mathrm{Re}(Z)\}^2 + \{\mathrm{Im}(Z_{el}) + \mathrm{Im}(Z)\}^2}} \tag{2.21}$$

where $\mathrm{Re}(Z_{el})$ and $\mathrm{Im}(Z_{el})$ are, respectively, the real and imaginary components of the complex impedance of the measuring device and Re(Z) and Im(Z) represent, respectively, the real and imaginary portions of the hydrophone's complex impedance. Assuming the loading of the measurement system is a parallel circuit of resistance R_L and capacitance C_L, the complex impedance components can be calculated as,

$$\mathrm{Re}(Z_{el}) = \frac{R_{el}}{1 + \omega^2 {R_{el}}^2 {C_{el}}^2} \tag{2.22}$$

and

$$\mathrm{Im}(Z_{el}) = \frac{-\omega {R_{el}}^2 C_{el}}{1 + \omega^2 {R_{el}}^2 {C_{el}}^2} \tag{2.23}$$

where ω is the angular frequency ($2\pi f$) and f is the frequency at the specified $M_c(f)$

If the impedance of the hydrophone and the load of the system are assumed to be capacitive, the end-of-cable sensitivity can be reduced to

$$M_L = M_C \frac{C_a}{C_a + C_c + C_s} \tag{2.24}$$

where C_a, C_c, and C_s are the capacitance of the sensitive element, the coaxial cable, and the stray capacitance, respectively. Figure 2.10 shows a schematic representation of this loading situation described in equation 2.24. The major loading on C comes from the cable capacitance C_c (typically 90 pF/m), which is much larger than the sensor capacitance, often on the order of 1 pF-3pF. Reducing the length of the cable is one way to decrease the impact of the cable capacitance on the hydrophone sensitivity. Other techniques to reduce the capacitive loading of the cable are to use a low-pass filter circuit or to incorporate a well designed preamplifier [4, 34].

Instead of presenting calibration data in terms of volts per MPa, end-of-cable voltage sensitivity is often expressed in decibels,

$$G_L(dB) = 20\log(M_L / M_{ref}) \tag{2.25}$$

where M_{ref} = 1V/Pa or 1 V/μPa [35].

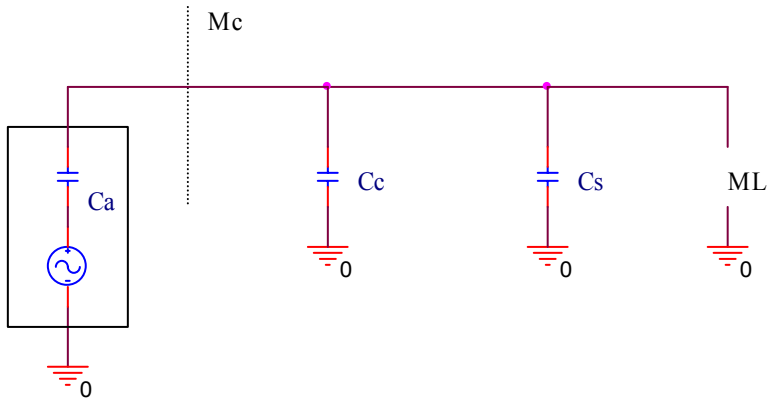

Figure 2.10: Schematic of line capacitance effect on the end-of-cable sensitivity.

2.2.4 Hydrophone calibration methods using Time Delay Spectrometry (TDS)

A brief review of the theory of Time Delay Spectrometry (TDS) is essential in order to understand its use with ultrasonic hydrophone calibration. A more detailed description of the TDS can be found in [36]. In an arbitrary electro-acoustic system, comprising a transmitter and receiver separated by a distance d, time delays (including the propagation time from the signal source to the receiver) can be converted into proportional shifts in instantaneous frequency. When the excitation signal from the transmitter is swept at a constant rate, the frequency shift is proportional to the time delay in the system.

Since transmission measurements are performed in a confined space such as a finite-sized water tank, there are several signals present, comprised of the one direct signal and the many reflected signal. The direct signal has the shortest traveling distance, which translates into a short propagation time as compared to the reflected signals. The longer propagation time for the reflected signals translates into a lower frequency than the direct signal. With the aid of an appropriate frequency-filtering scheme, the receiver will capture only the direct signal because of the presence of a shift in the instantaneous frequency. Therefore, with properly chosen parameters, the TDS technique would eliminate the effects of multiple transmission lines, standing waves, and other interferences due to the reflected signals, which means that TDS can create free-field conditions in a highly reverberant environment [35, 36, 37].

2.2.5 Substitution calibration method with Time Delay Spectrometry

A detailed outline of the ultrasonic hydrophone substitution calibration technique with TDS has been presented elsewhere [25, 35, 37]. A broadband ultrasonic transmitter, a reference hydrophone, and a spectrum analyzer are essential equipment used to perform this substitution calibration technique [25]. The initial step is to place the reference hydrophone in the far field of an ultrasonic transmitter that is operated by the tracking generator of the spectrum analyzer. Once the received signal of the hydrophone has been maximized, the frequency response of the reference hydrophone is stored in the memory of the spectrum analyzer. The received signal of the hydrophone is the frequency response of the entire electronic set-up (i.e., hydrophone, transmitter, and associated electronics).

The next step is to replace the reference hydrophone with the hydrophone to be calibrated and the same procedure is performed under the same conditions that applied for the reference hydrophone. A receive signal for the uncalibrated hydrophone is recorded once it has been maximized and is compared to the received signal of the reference hydrophone. The sensitivity of the hydrophone being calibrated M can now be determined by relating it to the sensitivity of the reference hydrophone M_{ref} and to the measured voltages [35]:

$$M = (U / U_{ref})M_{ref} \tag{2.26}$$

where U and U_{ref} are the terminal voltages of the uncalibrated hydrophone and the standard hydrophone, respectively.

Employing TDS allows a relatively quick hydrophone calibration since the frequency is swept over the frequency range of interest. This permits the hydrophone sensitivity to be determined as a virtually continuous function of frequency and displays any rapid variations in the frequency response that may be missed when measured at discrete frequency points [37]. A high signal-to-noise ratio is also achieved with the TDS procedure [28, 35, 36, 37].

CHAPTER 3.0: METHODOLOGY

This chapter discusses the design criteria of the wideband hydrophone preamplifier and programmable buffer assembly in the frequency range between 100 kHz and 40 MHz. Figure 3.1 provides a roadmap or an overview of the procedure in this work. The details of each part are explained in the following sections.

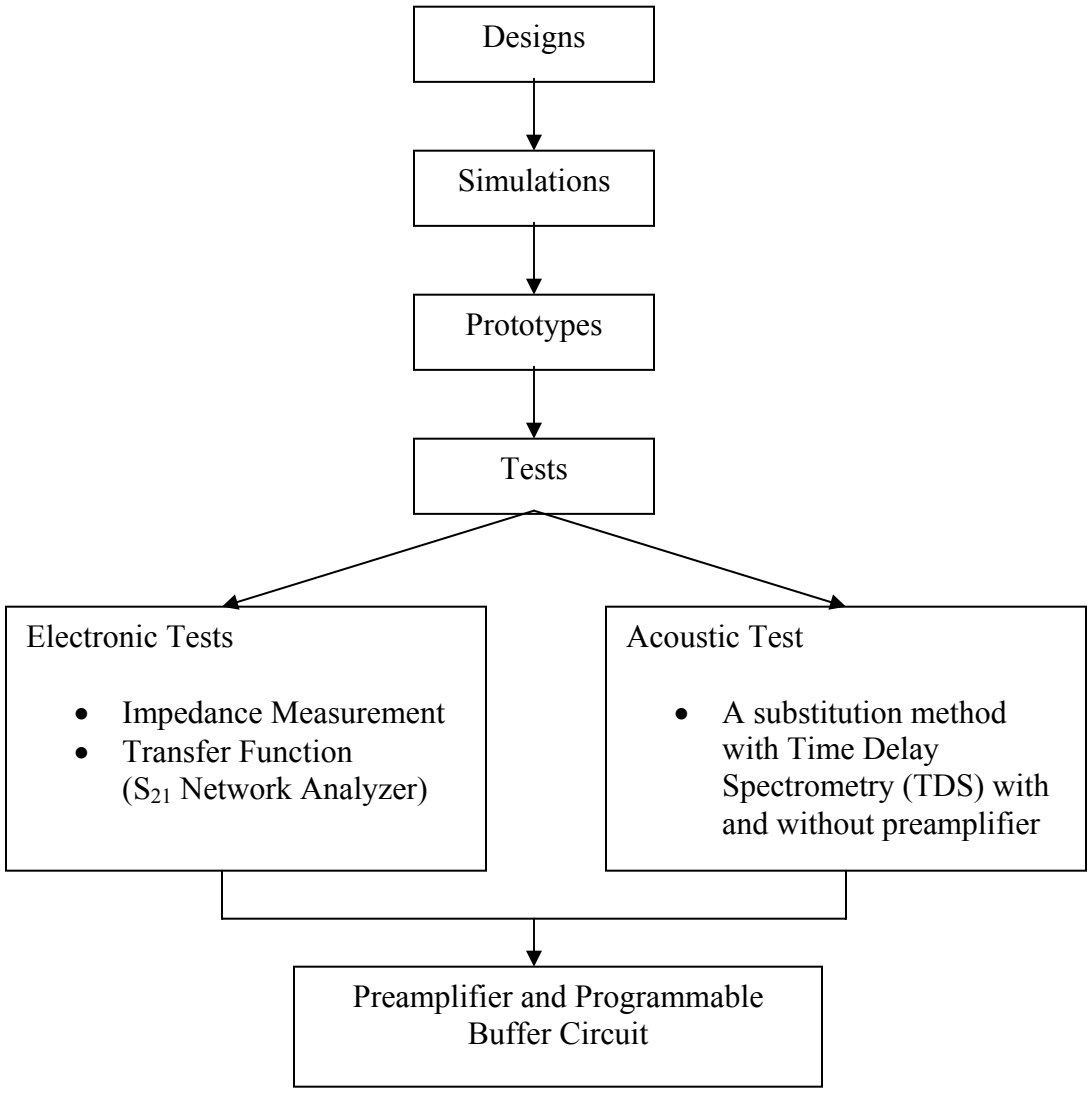

Figure 3.1: A roadmap or an overview of the procedure in this work.

3.1 Designs

The design constraints and general description of the preamplifier and the programmable buffer circuit are explained in sections 3.1.1 and 3.1.2.

3.1.1 Preamplifier

The preamplifier was designed with high input resistance (1MΩ), which minimizes loading of the hydrophone, and 50Ω output impedance to eliminate transmission line phenomena. The preamplifier requires a dual $\pm 5\,V$ power supply. The frequency response of the preamplifier was designed to comply with the Food and Drug Administration (FDA) requirements; the circuit operates between 100 kHz and 40 MHz. To optimize the performance in terms of input impedance, frequency response and dynamic range, the preamplifier was implemented in two stages using application specific operational amplifiers.

Instrumentation Amplifier topology was used to design the preamplifier because it ensured a high degree of accuracy when measuring low-level differential signals and had another major advantage that it offered high input impedance. The details of circuit topology of the preamplifier are shown in Figure 3.2.

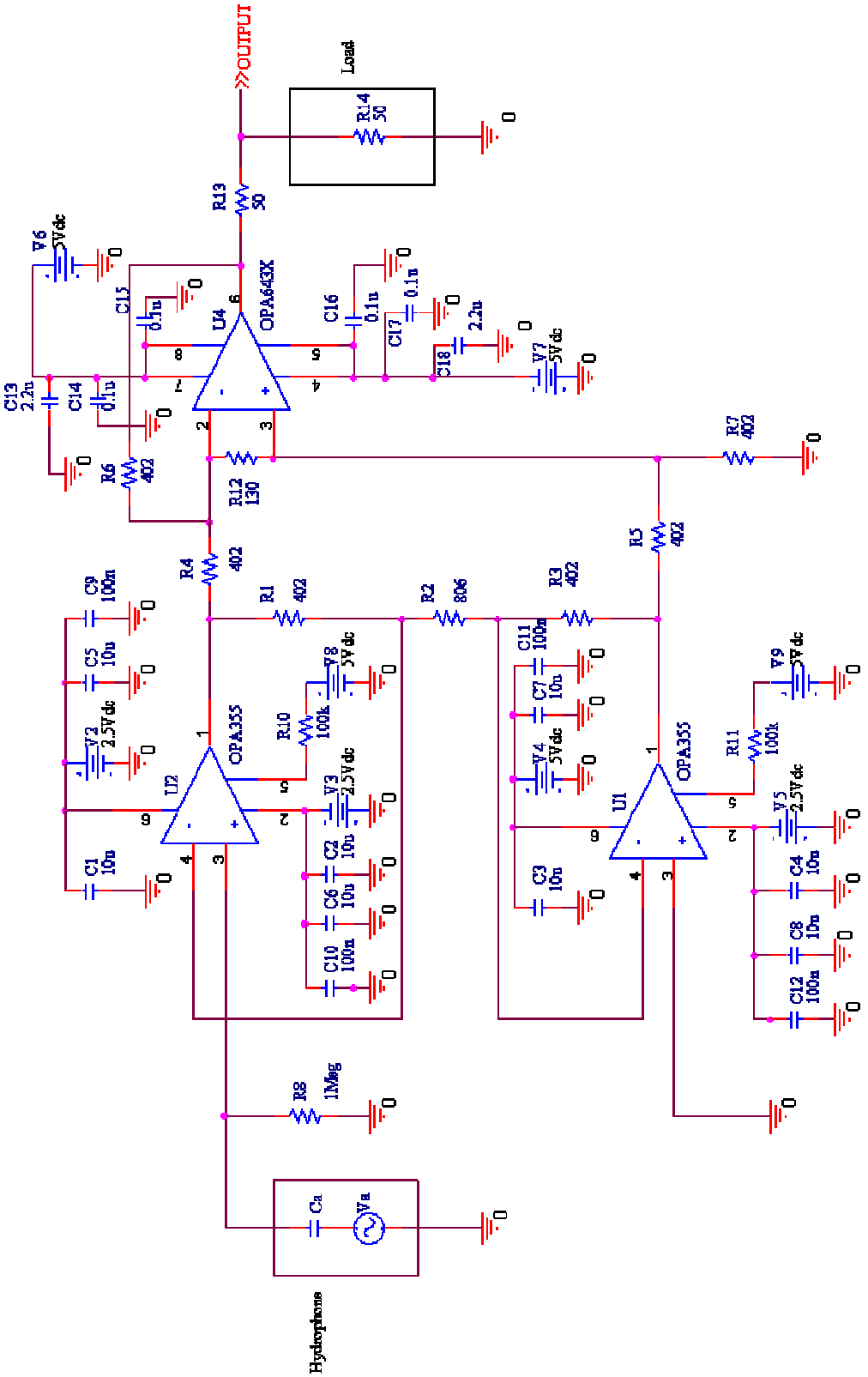

Figure 3.2: The circuit topology of the preamplifier

From Figure 3.2, the preamplifier circuit consists of two stages: The first stage is a buffered amplifier, which is formed by OP-AMPs U_1 and U_2, and their associated resistors (R_1, R_2 and R_3). The second stage is formed by a basic differential amplifier U_3 together with its four associated resistor (R_4, R_5, R_6 and R_7).

The input stage is realized with OPA355 (Burr-Brown Products from Texas Instruments). The OPA355 is a CMOS, high-speed, voltage feedback operational amplifier. It features a 200 MHz gain bandwidth, which is sufficient for the requirement (100 kHz-40 MHz) of this work. Since its slew rate is 360V/μs, the maximum input signal should not exceed 1.4V at 40 MHz. This maximum input signal value can be calculated from:

$$SlewRate(SR) \geq 2\pi f_{SR} V \tag{3.1}$$

where f_{SR} is the frequency at which an output sinusoid with amplitude equal to the rated output voltage of the OP-AMP begins to show distortion due to slew-rate limiting and the rated voltage is V.

Normally, the pressure amplitudes employed in diagnostic ultrasound imaging are approximately 10 MPa. Assume that the hydrophone's sensitivity is on the order of -260 dB re 1V/μPa. Therefore, the output voltage of the hydrophone is around 1V and then the slew rate limitation of OPA355 does not limit the input voltage signal.

Since the input-stage OP-AMP (OPA355) is specified over a power-supply range from $\pm 1.25\,V$ to $\pm 2.75\,V$ and to prevent OP-AMPs being used in saturation stage, the power supply of OPA355 in the preamplifier is $\pm 2.5\,V$. However, the preamplifier uses a dual $\pm 5\,V$ power supply. Therefore, the +5V needs to be fed through the positive voltage regulator PQ25EF01SZ, which generates +2.5V positive power supply to OPA355 and the -2.5V negative power supply of OPA355 comes from the output of the negative voltage regulator LT337AT. It was determined that $\pm 2.5\,V$ was sufficient to enable pressures up to 50 MPa to be measured. Such pressure is at least 4 times higher than those pressure amplitudes employed in therapeutic practice. To determine this it was assumed that the hydrophone's sensitivity is on the order of 100mV/MPa.

A 10μF ceramic bypass capacitor (C_1, C_2, C_3 and C_4) paralleled to a 10μF tantalum capacitor (C_5, C_6, C_7 and C_8) and a 100nF ceramic capacitor (C_9, C_{10}, C_{11} and C_{12}) on the power supply pin are essential to achieving very low harmonic and intermodulation distortion. They are also needed for stable operation.

The output stage is realized with OPA643 (Burr-Brown Products from Texas Instruments). The OPA643 provides a high level of speed and dynamic range (800MHz gain bandwidth), and achieves exceptionally low harmonic distortion over a wide frequency range. It also features high slew rate (1000V/μs), which ensures an adequate behavior with around $4V_{pp}$ input voltage (or 40 MPa) up to 40MHz (calculated from equation 3.1). It needs a power supply of $\pm 5\,V$, which is fed directly from the power supply of the preamplifier.

Although, the preamplifier design chosen here exhibits unity gain, the OPA643 is designed for a high gain operation. Decreasing the gain for the OPA643 from the nominal design point of 14 dB will decrease the phase margin. This will peak up the frequency response and extend the bandwidth. A peaked frequency response will show overshoot and ringing in the pulse response as well as a higher integrated output noise. Operating at a low noise gain also runs the risk of sustained oscillation (loop instability). To prevent those problems, therefore, the R_{12} resistor across the two inputs of OPA643 is necessary to be included in the preamplifier circuit. The R_{12} resistor increases the noise gain and decreases the loop gain without changing the signal gain. This approach retains the full slew rate and noise benefits to the output. The value of R_{12} suggested in the manufacturing data sheet is obtained from:

$$1 + R_6 /(R_4 // R_{12}) \geq +3 \tag{3.2}$$

The 0.1μF ceramic decoupling capacitors (C_{17}, C_{18}) and 2.2μF electrolyte capacitors (C_{13}, C_{14}) in parallel on the power supply pins (pins 4 and 7) are included in order to minimize the harmonic distortion. However, to deliver the lowest possible distortion of the output stage preamplifier, additional 0.1μF power supply decoupling capacitors on pin 5 and 8 of OPA643 is required as shown in Figure 3.2. Although pins 5 and 8 are internally connected to pins 4 and 7 respectively, the additional capacitors help to decouple the package lead inductances and decrease the second-harmonic distortion for a 5MHz fundamental by approximately 4 dB.

Since the output stage of the preamplifier is a voltage feedback OP-AMP, a wide range of resistor values may be used for the feedback and gain setting resistors (R_4, R_5, R_6 and R_7 in Figure 3.2). The primary limits to these values are set by dynamic range (noise and distortion) and parasitic capacitive consideration. From the OPA643 data sheet, the feedback resistor (R_6 and R_7) value should be between 200Ω and 1kΩ. Below 200Ω, the feedback network will present additional output loading which can degrade the harmonic distortion performance of the OPA643. Above 1kΩ, the typical parasitic capacitance (approximately 0.2pF) across the feedback resistors may cause unintentional band-limiting in the amplifier response. Therefore, the value of feedback resistors (R_6 and R_7) tested from the simulation in section 4.1, which is 402Ω, is set for the output stage of the preamplifier.

As already mentioned in section 2.1.2.4, the overall gain of the instrumentation amplifier can be calculated by the equation:

$$\frac{V_o}{V_s} = \left(1 + 2\frac{R_1}{R_2}\right)\frac{R_6}{R_4} \tag{3.3}$$

where R_1=R_3 and $R_5/R_4 = R_6/R_7$.

As already noted, the preamplifier described here was designed for an over all gain of one or equal to 0 dB (connected to 50Ω load). Therefore, from equation 3.3, the value of the feedback resistors (R6 and R7) above and the results from the simulation test with a few choices of different R's as shown in section 4.1, the optimum value of R_1, R_2, R_3, R_4, R_5,

R_6 and R_7 is 402, 806, 402, 402, 402, 402 and 402 Ohms, respectively. When the value of R_6 and R_4 is known, the value of R_{12} can be obtained from the equation 3.2: the value of R_{12} was calculated to be 130Ω.

Since the input-stage OP-AMP (U_2) is connected in the noninverting configuration and its input impedance is extremely high (10^{13}Ω//1.5pF), when connecting to 1 MegaOhms shunt resistor (R_8), the overall input impedance of the preamplifier is (ideally) 1 MΩ, while the 50Ω series resistor (R_{13}) at the output terminal provides a matching resistor for the measurement equipment load.

3.1.2 Programmable buffer circuit

The programmable buffer circuit designed to work with the hydrophone preamplifier operates also over the frequency range between 100 kHz and 40 MHz. It features 50Ω input impedance, which matches the source impedance of the test generator, and 50Ω output impedance to provide a matching resistor for the analyzing or measuring equipment load. The programmable buffer circuit requires dual ± 10 V power supply. Visual Basic programming was employed to automatically execute On/Off function. When the programmable buffer circuit and the preamplifier are combined together and controlled via LabVIEW programs, the implemented circuit topology allows fully automatic determination of key acoustic output parameters of diagnostic ultrasound scanners, which determine the safety indicators such as Mechanical Index (MI) and Thermal Index (TI).

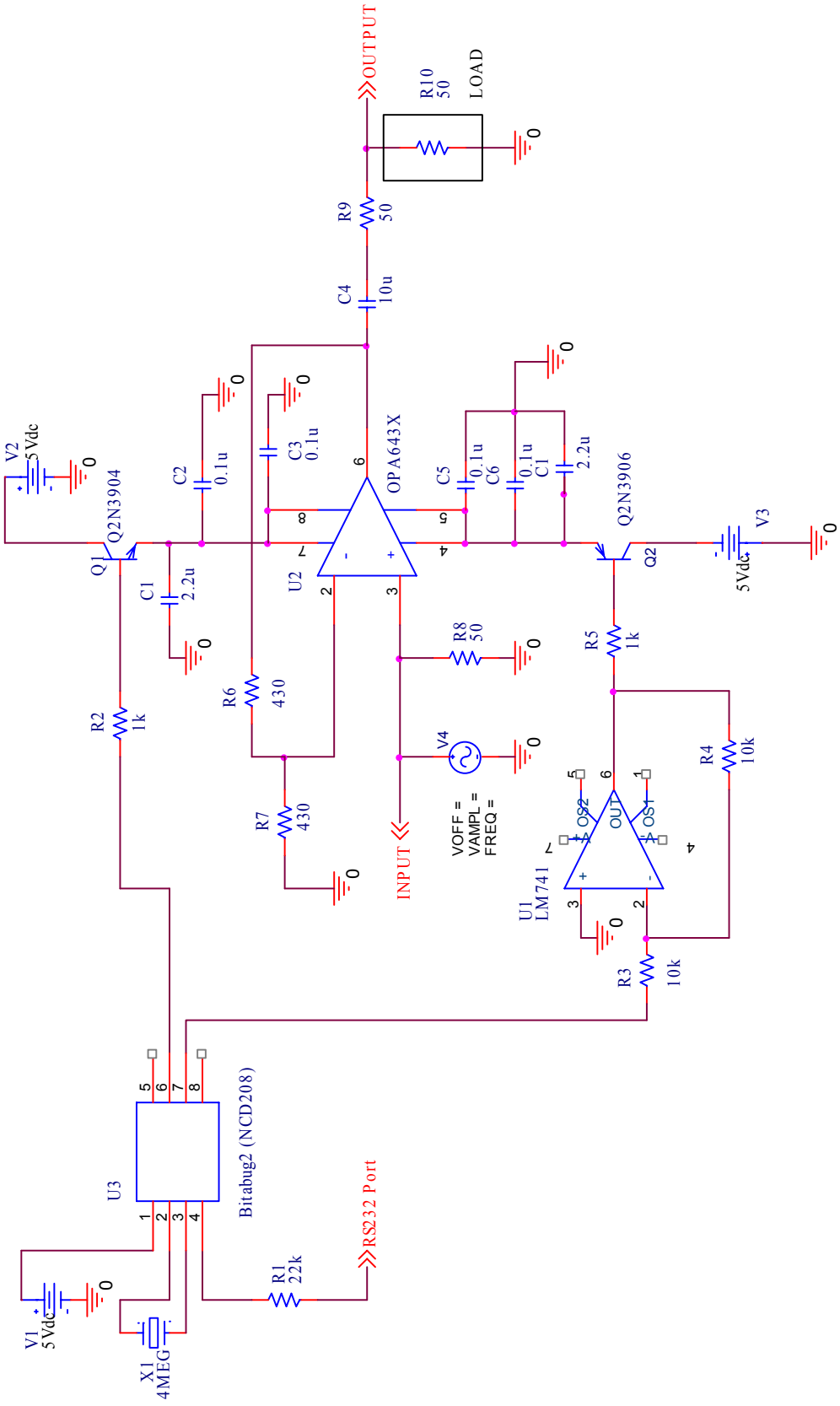

Figure 3.3: The circuit topology of the programmable buffer circuit

The programmable buffer circuit consists of two stages: The first stage is a controller stage which is formed by a Bitabug2 controller (NCD208), an inverting amplifier U1 (LM741), a PNP transistor (Q2N3906), an NPN transistor (Q2N3904) and their associated resistors (R1, R2, R3, R4 and R5) . The second stage is formed by a buffer amplifier U_2 (OPA643) together with its four associated resistor (R_6, R_7, R_8 and R_9). The circuit topology of the programmable buffer circuit is shown in Figure 3.3.

As noted above, the first stage is realized with Bitabug2 or NCD208 controller (National Control Devices Products). Bitabug2 is an 8-pin preprogrammed microcontroller. It is programmed as a 3-bit serial-to-parallel converter, and will only respond to incoming ASCII character codes in the range of 0 to 7. Visual Basic programming was employed to automatically execute On/Off function by sending ASCII character code 0 for Off and code 3 for On. These data are transferred via the RS232 serial port to Bitabug2. The description of Visual Basic programming source code is explained in Appendix B.

Bitabug2 requires a regulated +5V power supply but the power supplies of programmable buffer circuit are ± 10 V. Therefore, a +5V voltage regulator (NJM7805FA) and a -5V voltage regulator (NJM7905FA) must be included in the circuit.

Bitabug2 has three TTL/CMOS (0/+5 volt) outputs, which are driven under computer control. However, only two outputs from Bitabug2 are used in the programmable buffer circuit and these outputs are controlled by Visual Basic programming. If the programmable buffer circuit is On, both outputs from Bitabug2 are “High” (+5V) but if it

is Off, both outputs are “Low” (0V). One of the outputs from Bitabug2 is connected directly to a NPN transistor (Q2N3904) and the other is connected through the inverting amplifier (LM741), to invert the output of Bitabug2 from +5V to -5V, into a PNP transistor (Q2N3906). The two transistors Q2N3904 and Q2N3906 operate as a switch between power supply of the OPA643 and its power supply pin in order to control On/Off of the programmable buffer circuit.

To prevent the output of inverting amplifier (LM741) to become saturated and obtain the output $-5\,\mathrm{V}$, the power supply fed in LM741 is $\pm 9\,\mathrm{V}$, which comes from the voltage regulator NJM7809FA and NJM7909FA. The output voltage -5V from LM741 is needed in order to have enough current to bias transistor Q2N3906.

The second stage of the programmable buffer circuit is implemented with OPA643 (Burr-Brown Products from Texas Instruments), which is exactly the same OP-AMP as the output stage of the preamplifier. As already mentioned in the section 3.1.1, the OPA643 features high bandwidth (800MHz) and high slew rate (1000V/μs). It is connected in the noninverting configuration with 0 dB gain (connected to 50Ω load) and requires $\pm 5\,\mathrm{V}$ power supply. However, again as the power supply of the programmable buffer circuit is $\pm 10\,\mathrm{V}$, positive (NJM7805FA) and negative (NJM7905FA) voltage regulators are required to obtain the desired voltage.

The 50Ω shunt resistor (R_8) at the input terminal matches the source impedance of the test generator, while the 50Ω series resistor (R_9) at the output terminal provides a matching resistor for the measuring and analyzing equipment load.

The 0.1μF ceramic decoupling capacitors (C_2, C_3, C_5 and C_6) and 2.2μF electrolyte capacitors (C_1, C_7) in parallel on the power supply pin are connected in order to deliver the lowest harmonic distortion. A 10μF tantalum capacitor (C_4) filters the DC signal from the OPA643.

3.2 Simulations

After the circuit topologies in Figure 3.2 and 3.3 were designed, the simulation was carried out to verify that those circuits would work satisfactorily before prototyping. Also, several choices of the different sets of feedback resistors in the preamplifier circuit topology in Figure 3.2 were simulated in order to show the optimum values of the design. Therefore, Pspice simulation program was used for numerical analysis of the circuits in Figure 3.2 and 3.3. The simulation results including transfer function characteristics in both magnitude (in dB) and phase (in degree) of the preamplifier and programmable buffer circuit are discussed in section 4.1.

3.3 Prototypes

After the circuit topologies in Figure 3.2 and 3.3 were verified using Pspice circuit simulation, the prototyping process started. To achieve optimum performance with high frequency operation, the prototypes of preamplifier and programmable buffer circuit required careful attention to board layout and external component types in order to minimize parasitic effects. The optimization of the layout was achieved by minimizing the distance between pins and the capacitors, careful selection and placement of external components, and no socketing in these high speed OP-AMPs. These procedures are explained in more detail in the Appendix C.

3.4 Experimental Test

This section described acoustic and electronic tests carried out to determine the performance of the preamplifier and programmable buffer assembly. The electronic test (section 3.4.1) determined the impedance and transfer function (S_{21}). The acoustic test in section 3.4.2 was performed during actual calibration of hydrophones with Time Delay Spectrometry (TDS).

3.4.1 Electronic test

The electronic test employed advanced measurement techniques for determining the preamplifier's and programmable buffer circuit's key characteristics as described in the following:

3.4.1.1 Impedance Measurement

The electrical impedance (Z) and admittance (Y) of the preamplifier and programmable buffer circuit were measured in the frequency range of 100 kHz to 40 MHz at discrete intervals using the Agilent 4395A Impedance Analyzer and the Agilent 43961A RF Impedance test kit. These measurements provided both the magnitude and phase of the programmable preamplifier. Figure 3.4 shows a schematic of the impedance measurement set-up for the preamplifier and programmable buffer circuit.

The impedance of the membrane and needle type hydrophone was also measured in order to compare the impedance between the preamplifier and the hydrophone. This was done to verify that the input impedance of the preamplifier was high enough in order to minimize loading of the hydrophone. The admittance measurement was used to determine the thickness resonance of the piezoelectric materials of the hydrophones. However, the measurement set-up of the preamplifier, programmable buffer circuit and hydrophones was almost the same except the hydrophone was immersed in water. Figure 3.5 shows a measurement set-up for determining hydrophone impedance.

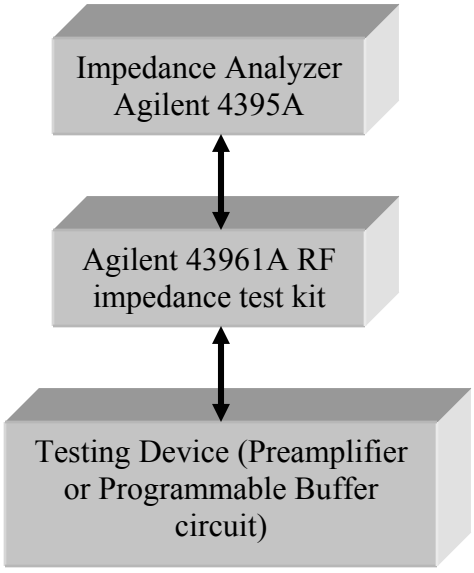

Figure 3.4: A schematic of the impedance measurement set-up for the preamplifier and programmable buffer circuit.

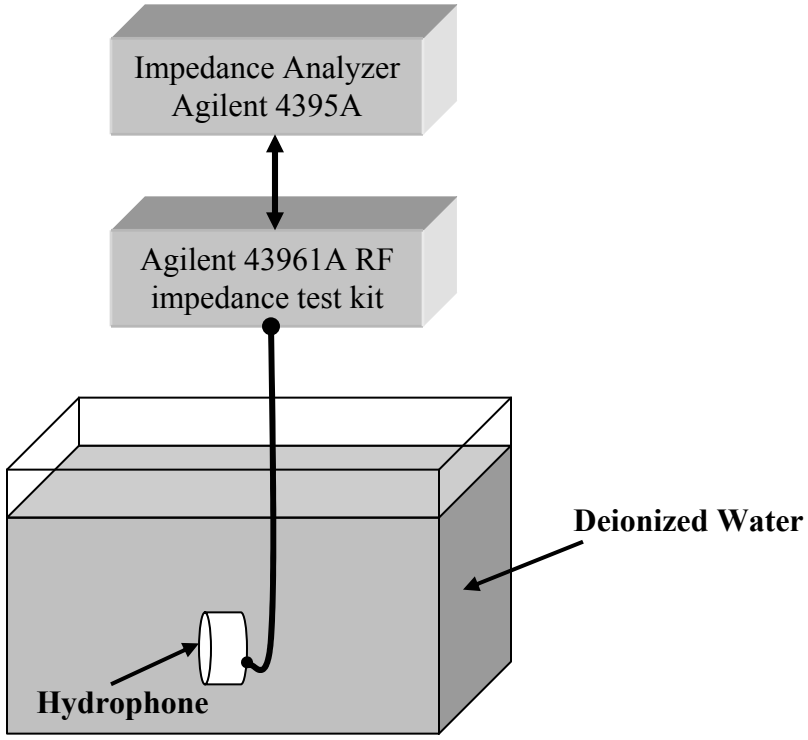

Figure 3.5: Measurement set-up for determining hydrophone impedance.

3.4.1.2 Transfer Function (S_{21}) Measurement

The Scattering parameter S_{21} (transfer function) was measured to identify the electrical characteristics of the preamplifier and the programmable buffer circuit. The Agilent 4395A Network Analyzer was used to measure S_{21} parameter in the frequency range of 100 kHz to 40 MHz at 200 kHz intervals. This provided transfer function characteristics of the testing device in terns of magnitude (in dB) and phase (in degrees). Figure 3.6 shows a schematic of the S_{21} measurement set-up for the preamplifier and programmable buffer circuit.

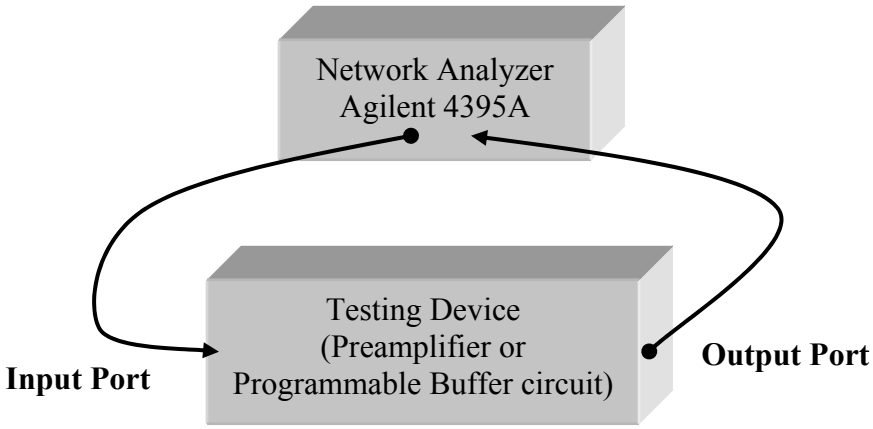

Figure 3.6: A schematic of the S_{21} measurement set-up for the preamplifier and programmable buffer circuit.

3.4.2 Acoustic test

Figure 3.7 shows the acoustic measurement test setup employed in this study. A swept frequency signal, which originates from the tracking generator of the spectrum analyzer HP 3583A, is controlled On/Off by the custom-built programmable buffer circuit. The output signal of the programmable buffer circuit is amplified by the ENI power amplifier and this amplifier signal is subsequently used to drive the ultrasonic transmitter. The IBM PC computer collects the measurement data and analyzes the results for the hydrophone calibration with a customized LabVIEW program. Deionized water was used and the water temperature during calibration was constant to within 0.5°C.

The execution of the substitution calibration method with TDS was conducted using the measurement setup as shown in Figure 3.7. With the ultrasonic source transducer and the reference hydrophone placed immersed in the water tank, the reference hydrophone was positioned in the far field region of the acoustic source using the X-Y-Z micro-manipulator. The signal, which represents the frequency response of the transmitter and calibrated reference hydrophone, was captured by the spectrum analyzer and then stored in the computer using LabVIEW program.

After the frequency response of the working reference hydrophone was established and stored, the hydrophone being calibrated replaced the reference hydrophone in the water tank. The test configuration and procedure for this step was the same as in the previous step. The combined frequency response of the hydrophone needing calibration and

ultrasonic transducer was stored in another file in the computer once its signal had been maximized by optimizing their orientation. The difference of the two frequency responses was taken and this difference represented the free field hydrophone frequency response of the hydrophone undergoing calibration [37]. By comparing the difference to the absolute sensitivity of the reference hydrophone, the voltage sensitivity of the hydrophone being calibrated was obtained.

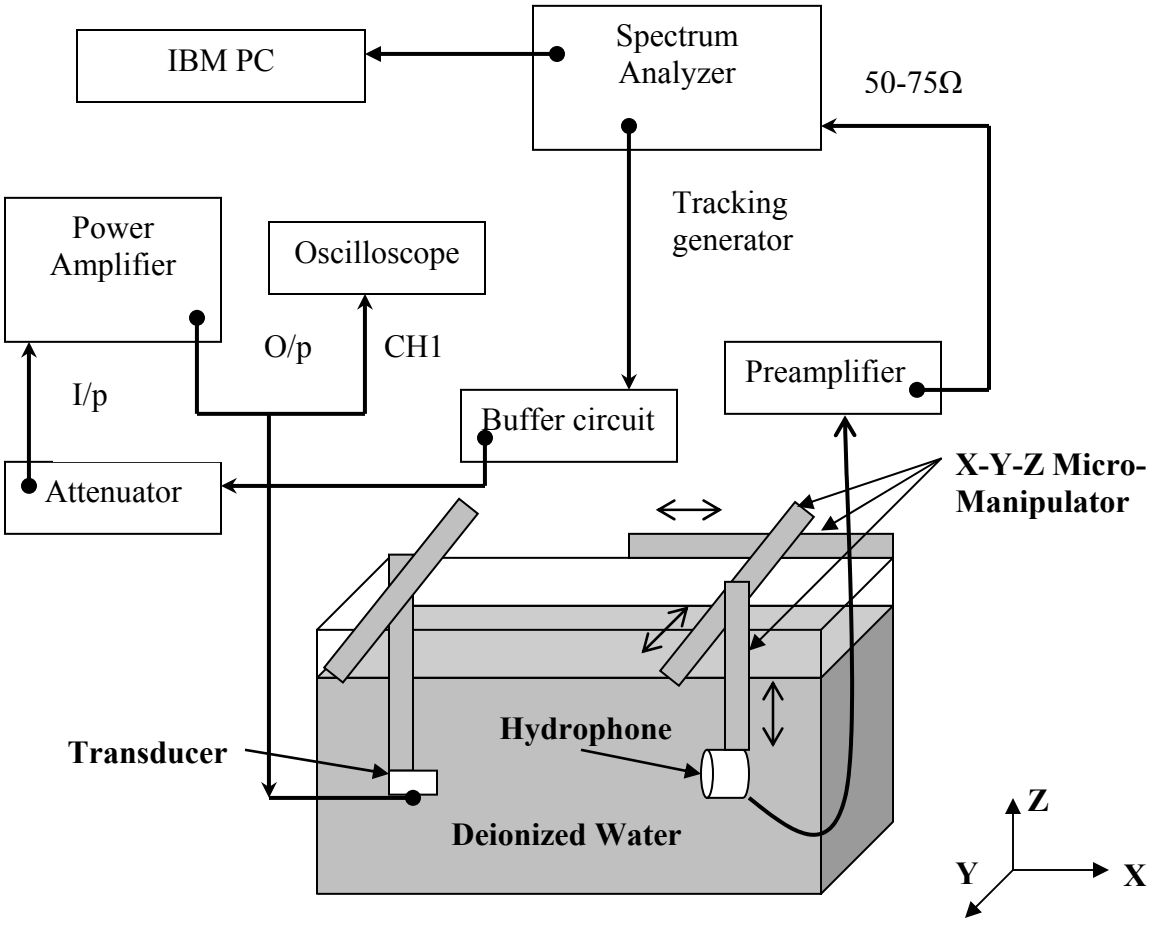

Figure 3.7: The setting for an acoustics test measurement.

CHAPTER 4.0: RESULTS

This chapter presents the results from the simulations, prototyping and tests outlined in the previous chapter.

4.1 Simulation Results

Three different sets of feedback resistors in the preamplifier circuit topology in Figure 3.2 were simulated in order to show the optimum values. The first set of the feedback resistors (R_f 402 Ohms in the Figure 4.1) is composed of R_1, R_2, R_3, R_4, R_5, R_6 and R_7 having values 402, 806, 402, 402, 402, 402 and 402 Ohms, respectively. The second set (R_f 1 kOhms in the Figure 4.1) consists of R_1, R_2, R_3, R_4, R_5, R_6 and R_7 with values 1k, 2k, 1k, 1k, 1k, 1k and 1k Ohms, respectively. Finally, the third set (R_f 200 Ohms in the Figure 4.1) is composed of R_1, R_2, R_3, R_4, R_5, R_6 and R_7 having values 200, 400, 200, 200, 200, 200 and 200 Ohms, respectively. The value of R_1, R_2, R_3, R_4, R_5, R_6 and R_7 in each set came from equation 3.3 detailed in section 3.1.1. The transfer function results of these three sets are shown in terms of magnitude and phase in Figure 4.1 and 4.2, respectively. That the magnitude of the transfer function of the Pspice simulation should be closet to 0 dB gain was the criterion to determine the optimum set of resistors.

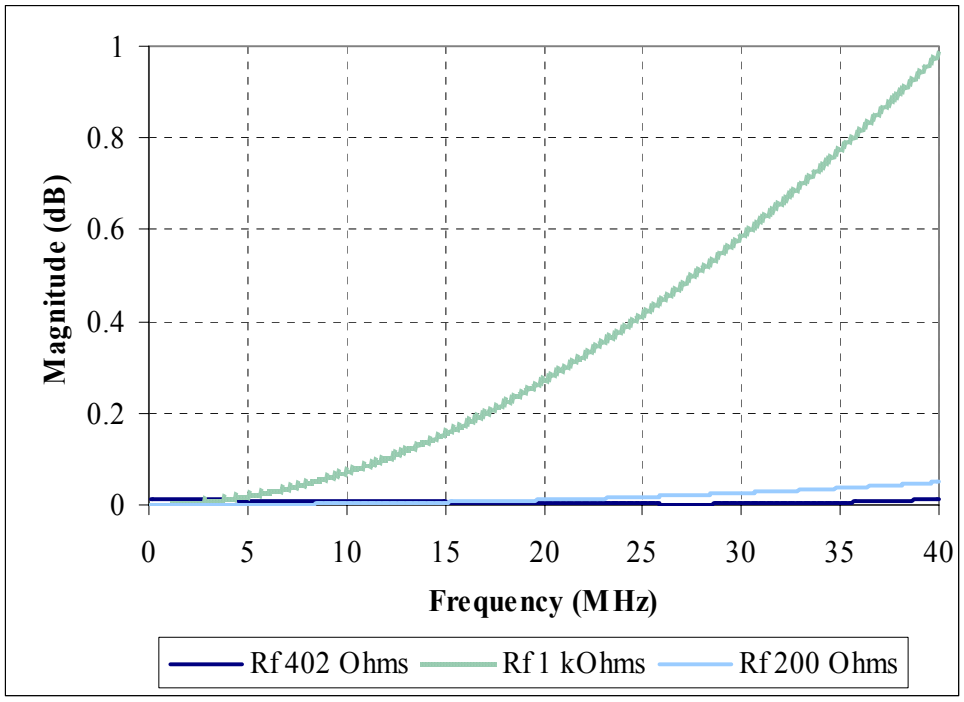

Figure 4.1: The transfer function of the preamplifier in term of magnitude (dB) from Pspice simulation when varying the different sets of resistors.

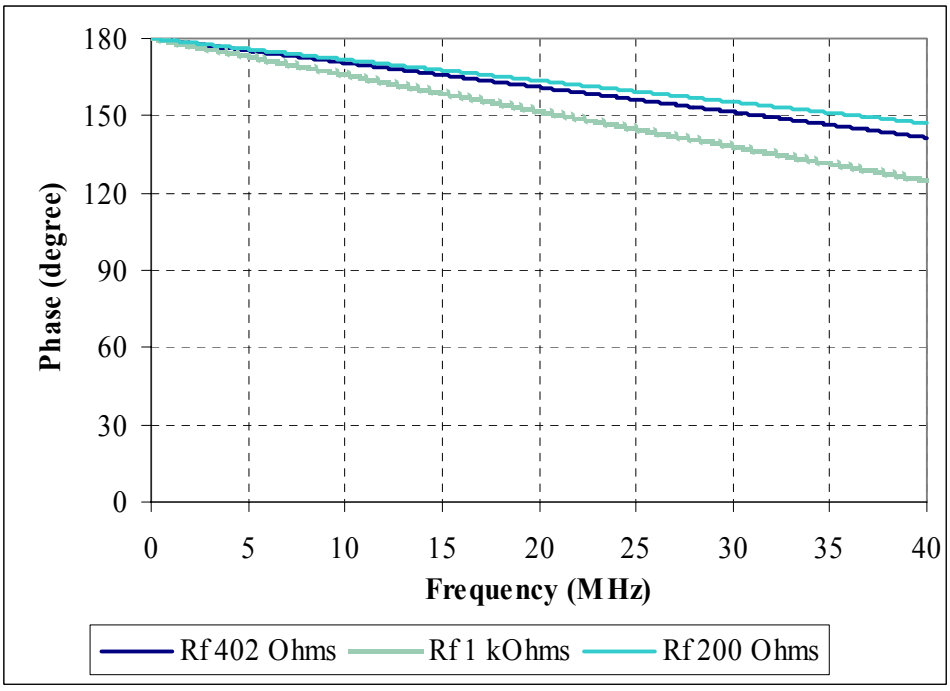

Figure 4.2: The transfer function of the preamplifier in term of phase (degree) from Pspice simulation when varying the different sets of resistors.

After the optimum resistor values are obtained from results in Figure 4.1 and 4.2, the transfer function of the optimized resistors was plotted again with a better scale to present its result clearly as shown in Figure 4.3 and 4.4. Also, the results from Pspice Simulations of the circuit topologies in 3.3 are shown in Figure 4.5 and 4.6. These simulations yielded the transfer function characteristics of the preamplifier and programmable buffer circuit in terms of magnitude (dB) and phase (degree).

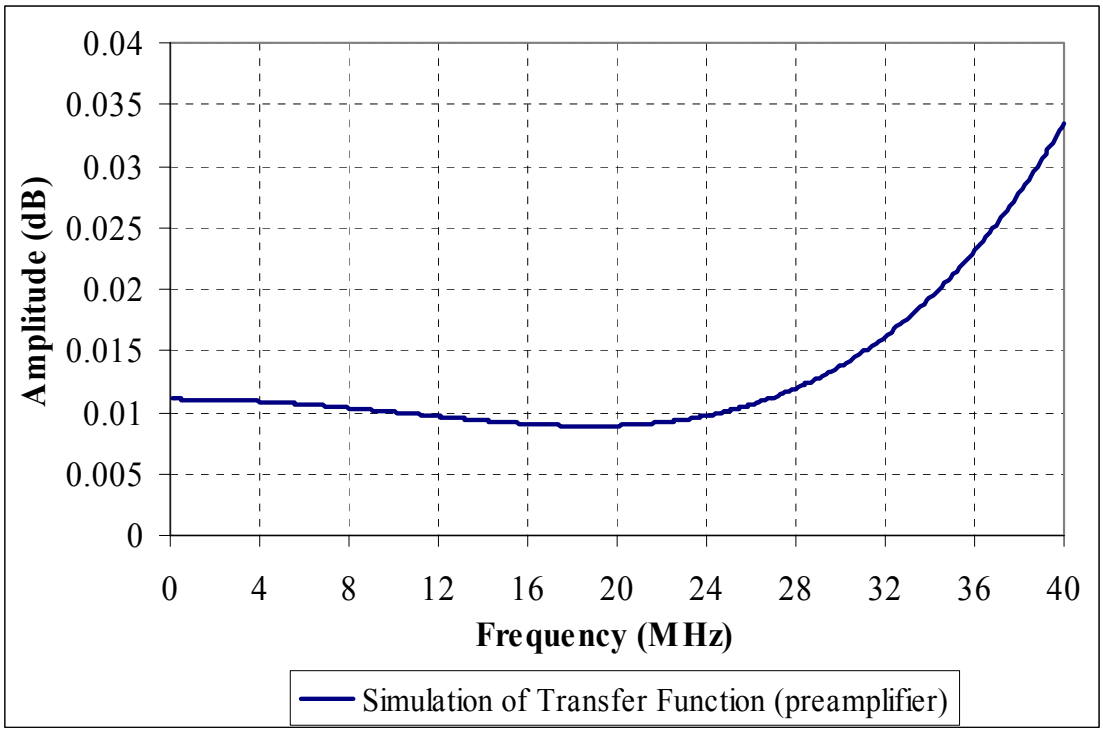

Figure 4.3: The transfer function of the optimum feedback resistors of the preamplifier in terms of magnitude (dB) from Pspice simulation.

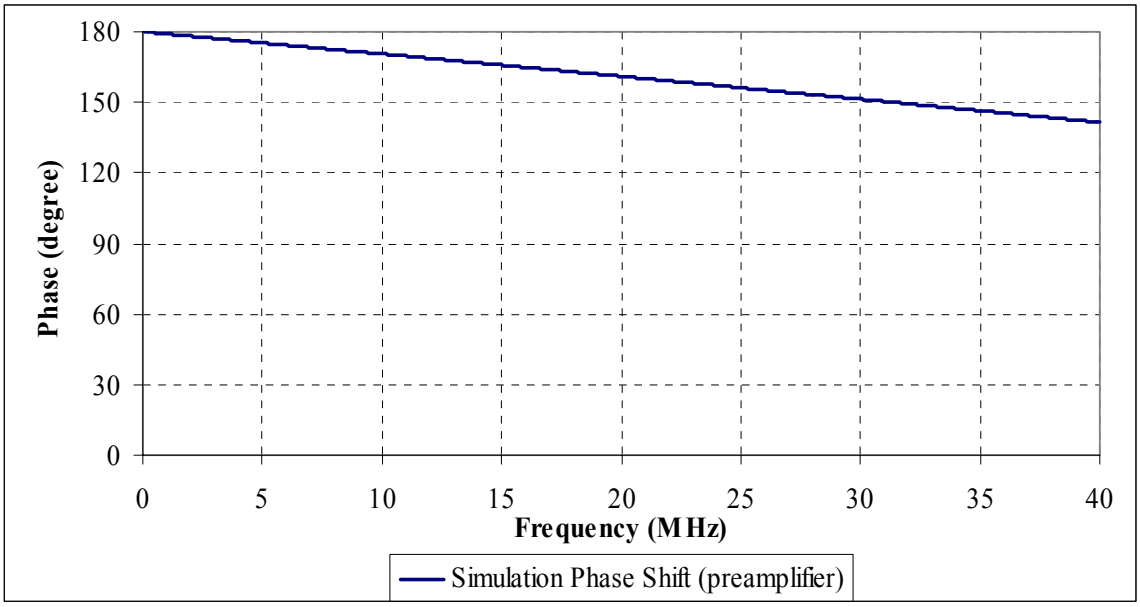

Figure 4.4: The transfer function of the optimum feedback resistors of the preamplifier in terms of phase (degree) from Pspice simulation.

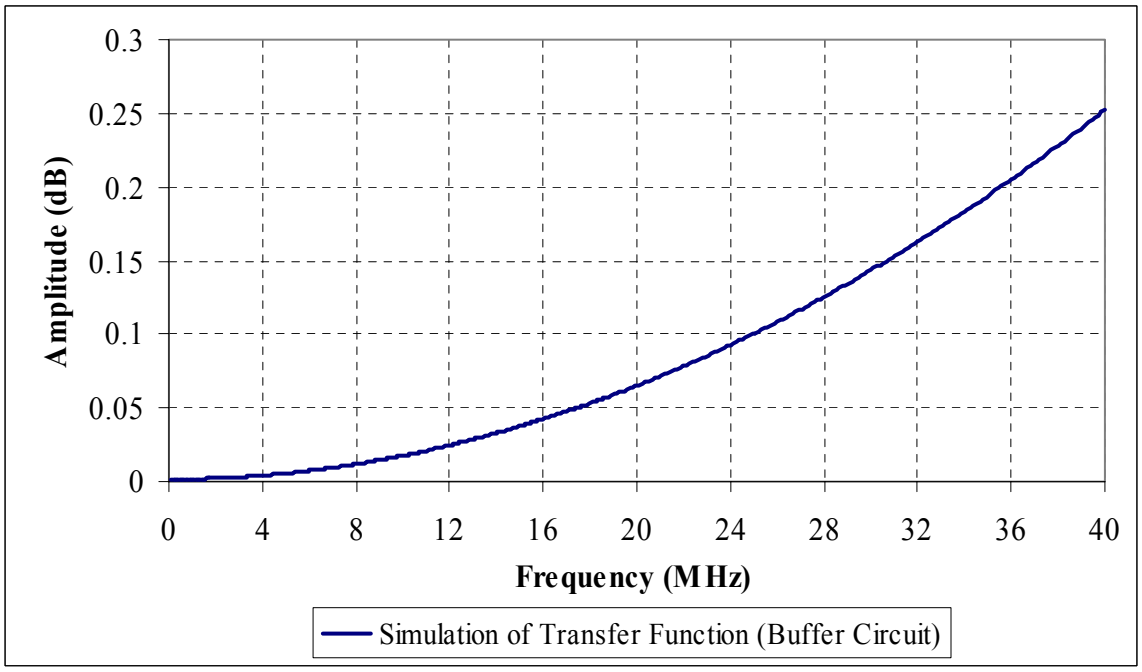

Figure 4.5: The transfer function of the programmable buffer circuit in terms of magnitude (dB) from Pspice simulation.

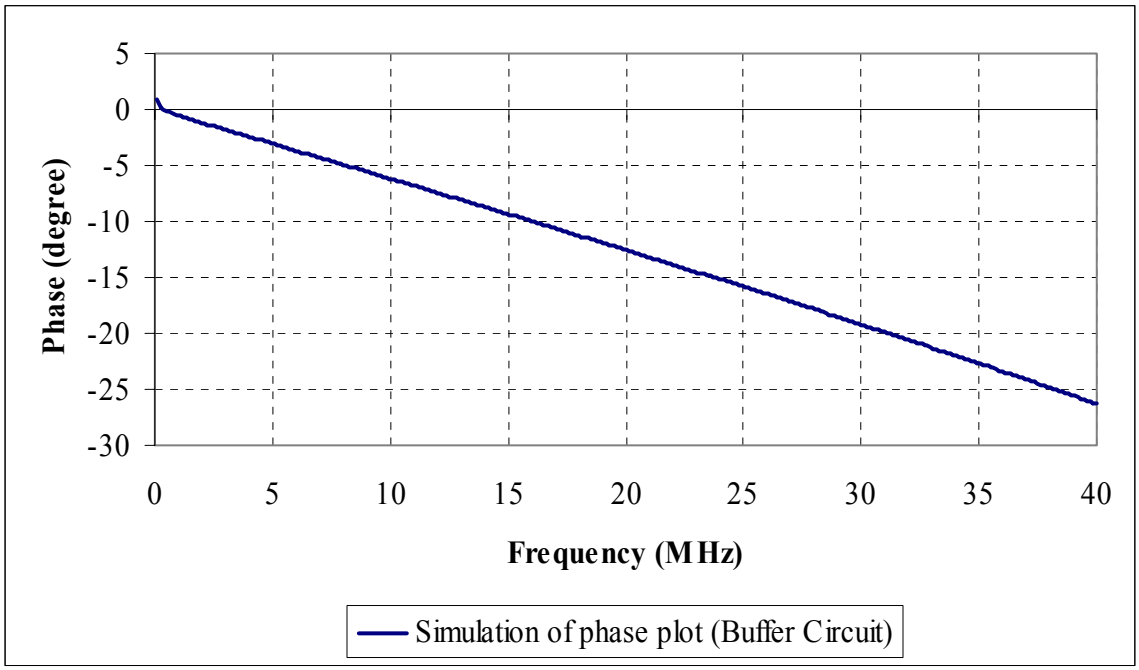

Figure 4.6: The transfer function of the programmable buffer circuit in terms of phase (degree) from Pspice simulation.

4.2 Prototyping Results

After the circuit topologies shown in Figures 3.2 and 3.3 were verified by the Pspice simulation, the prototypes of the preamplifier and programmable buffer circuit were built; these prototypes are shown in Figure 4.7.

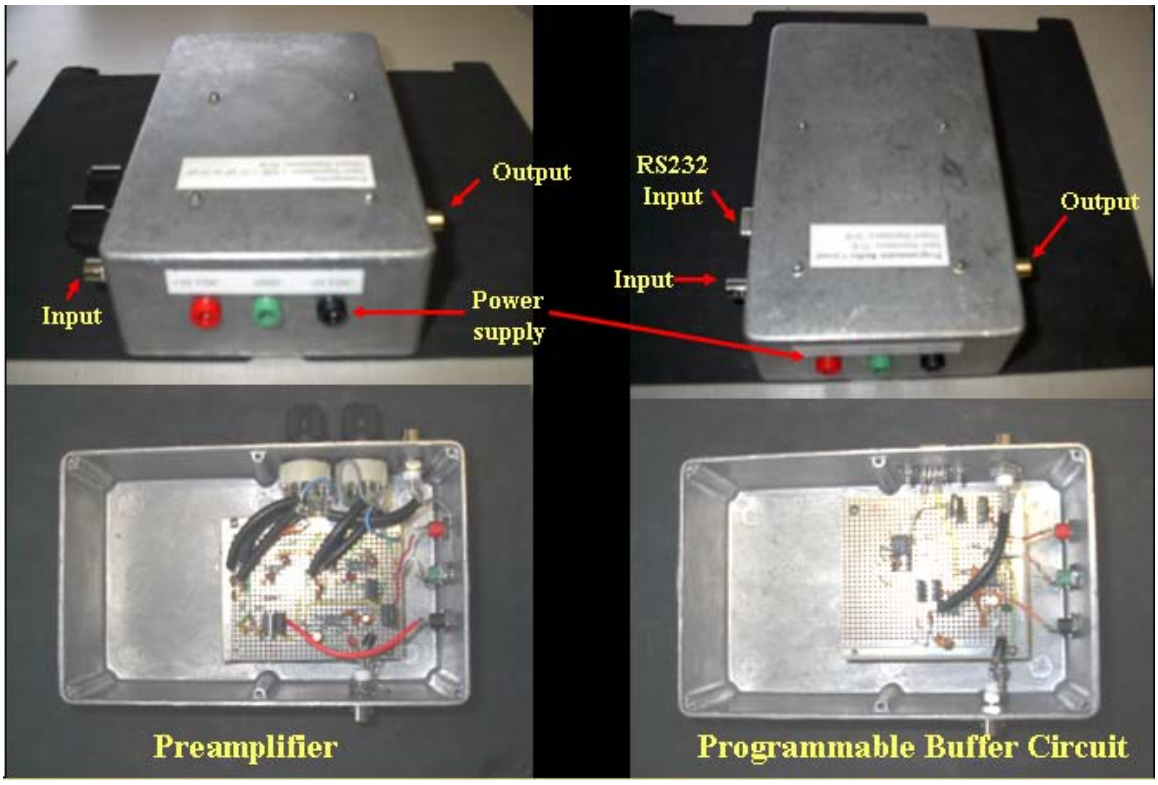

Figure 4.7: The prototypes of preamplifier and programmable buffer circuit.

4.3 Experimental Results

4.3.1 Impedance Measurement

The input impedance, Z, of the prototyping preamplifier, needle type hydrophone and membrane type hydrophone were measured in the frequency range of 100 kHz to 40 MHz at 200 kHz intervals as shown in Figure 4.8 (magnitude) and 4.9 (phase). These results are shown for comparison in order to verify that the input impedance of the preamplifier was sufficiently high so the loading of the hydrophone could be minimized.

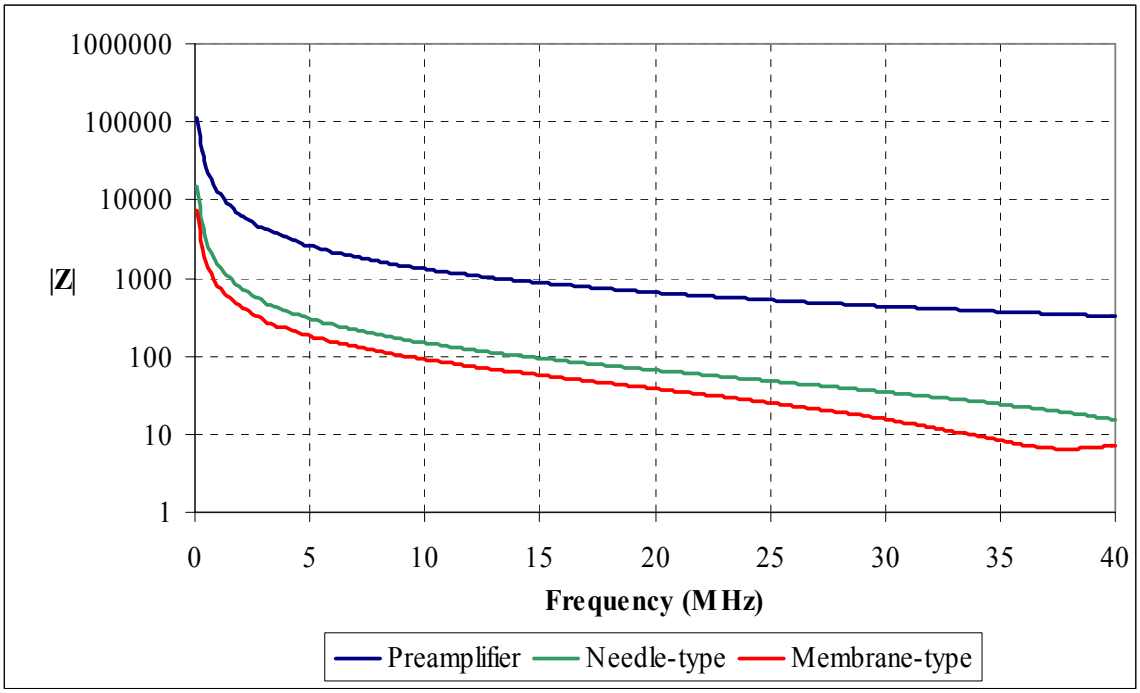

Figure 4.8: Comparison of the (magnitude) impedance of the preamplifier to the needle-type and membrane type hydrophones.

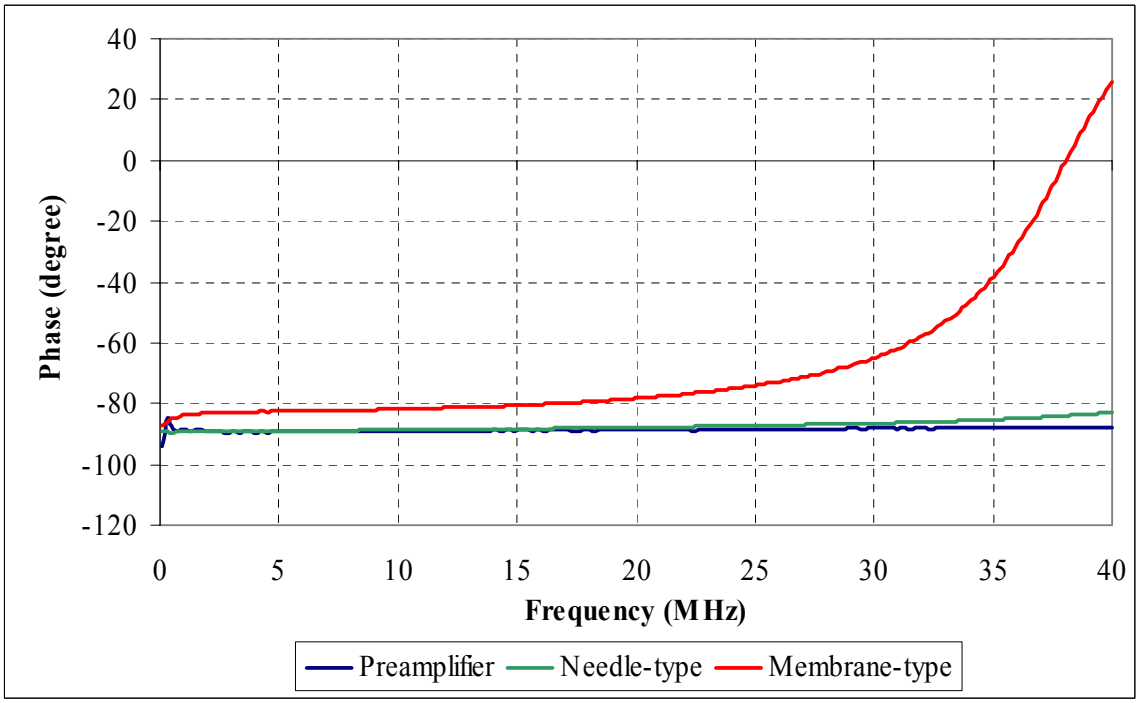

Figure 4.9: Comparison of (phase) impedance of the preamplifier to the needle-type and membrane type hydrophones.

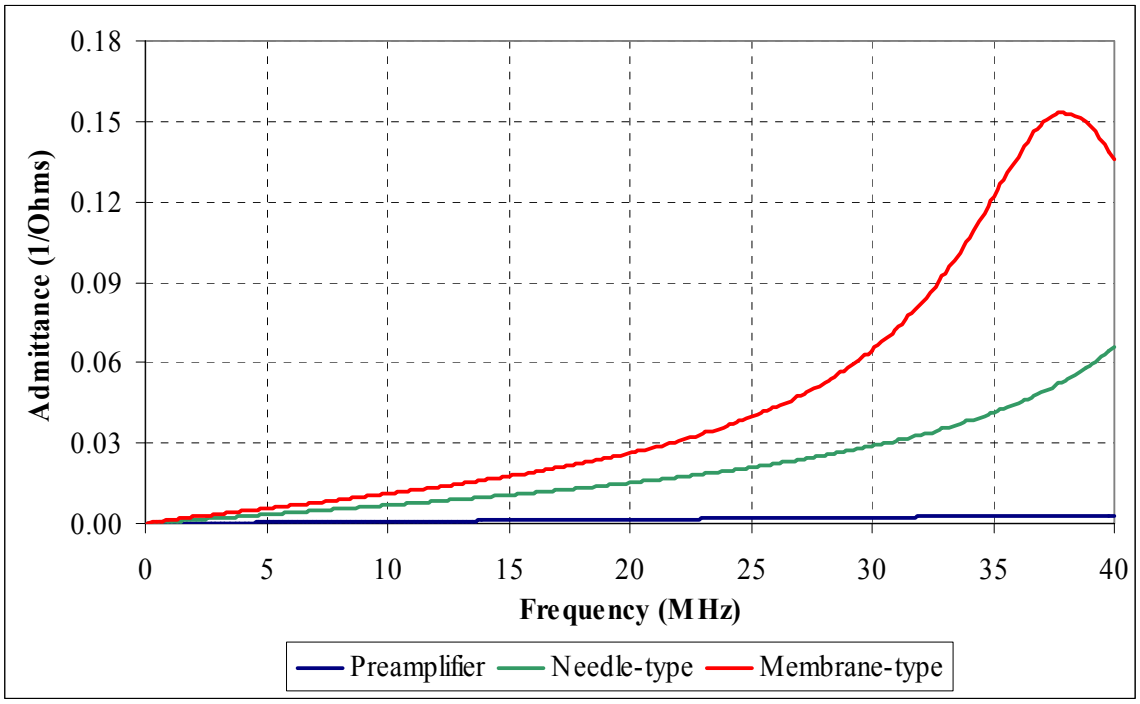

Figure 4.10: The admittance (magnitude) measurement of preamplifier, needle-type and membrane-type hydrophone.

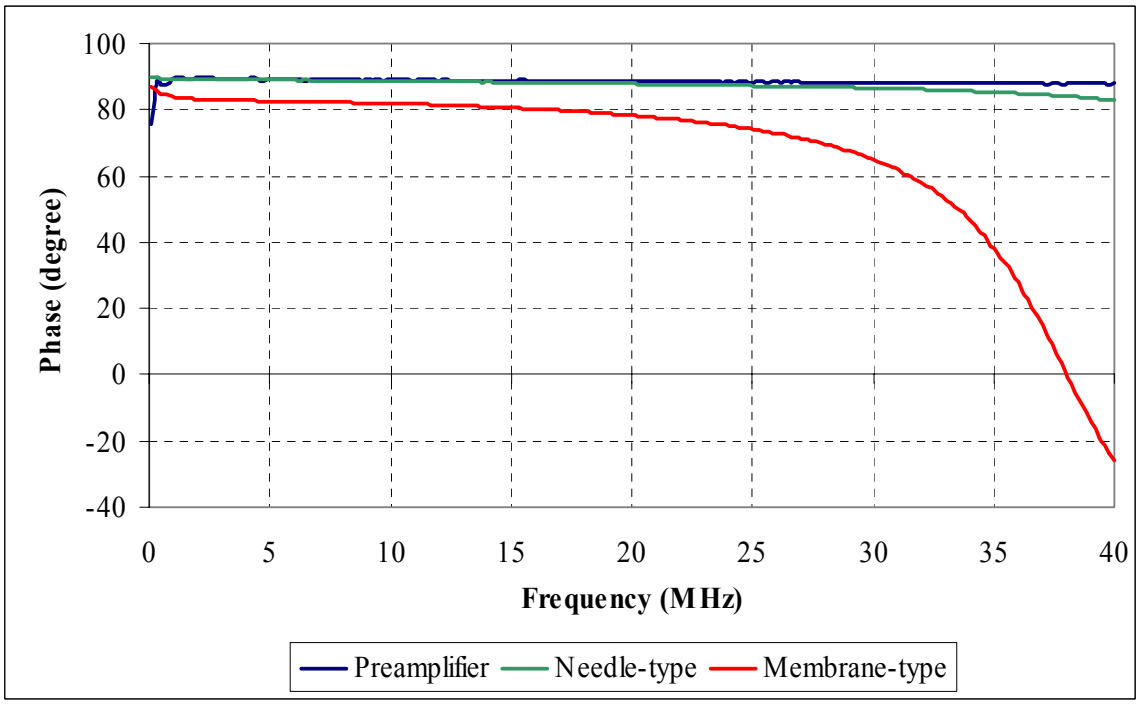

Figure 4.11: The admittance (phase) measurement of preamplifier, needle-type and membrane-type hydrophone.

Figure 4.10 and 4.11 show the results of the admittance measurement, which were used to determine the thickness resonance of the piezoelectric materials of the hydrophones.

4.3.2 Transfer Function (S_{21}) Measurement

The Scattering parameter S_{21} measurement was used to measure the transfer function characteristics of the preamplifier and programmable buffer circuit in the frequency range from 100 kHz to 40 MHz at 200 kHz intervals. The results of this measurement are shown in Figure 4.12-4.15.

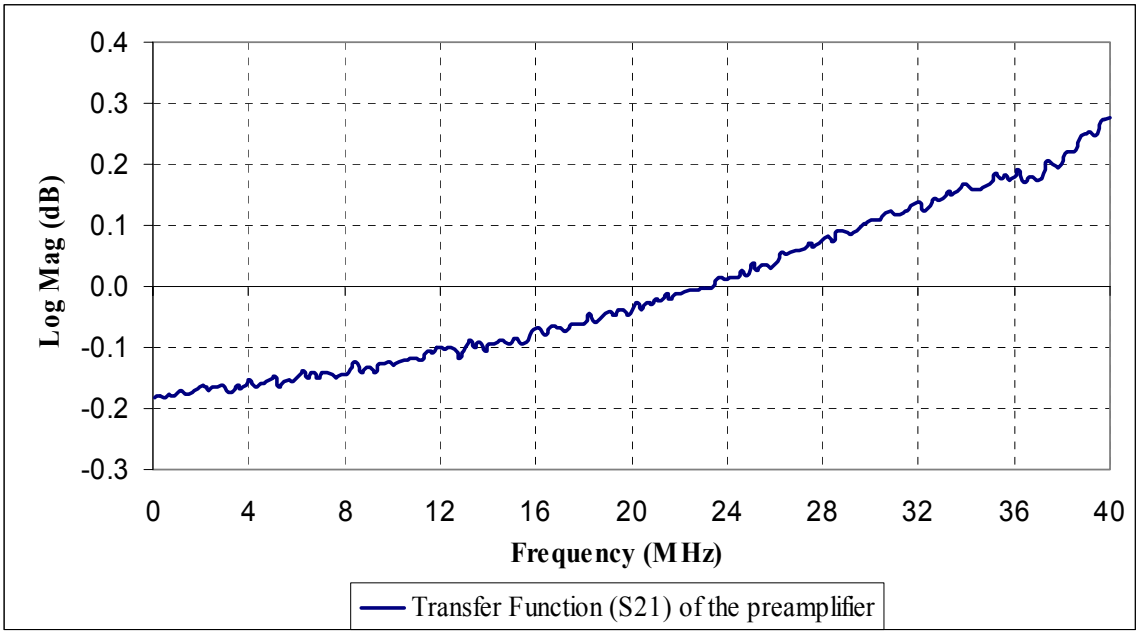

Figure 4.12: The transfer function (S_{21}) of the preamplifier in terms of magnitude (in dB).

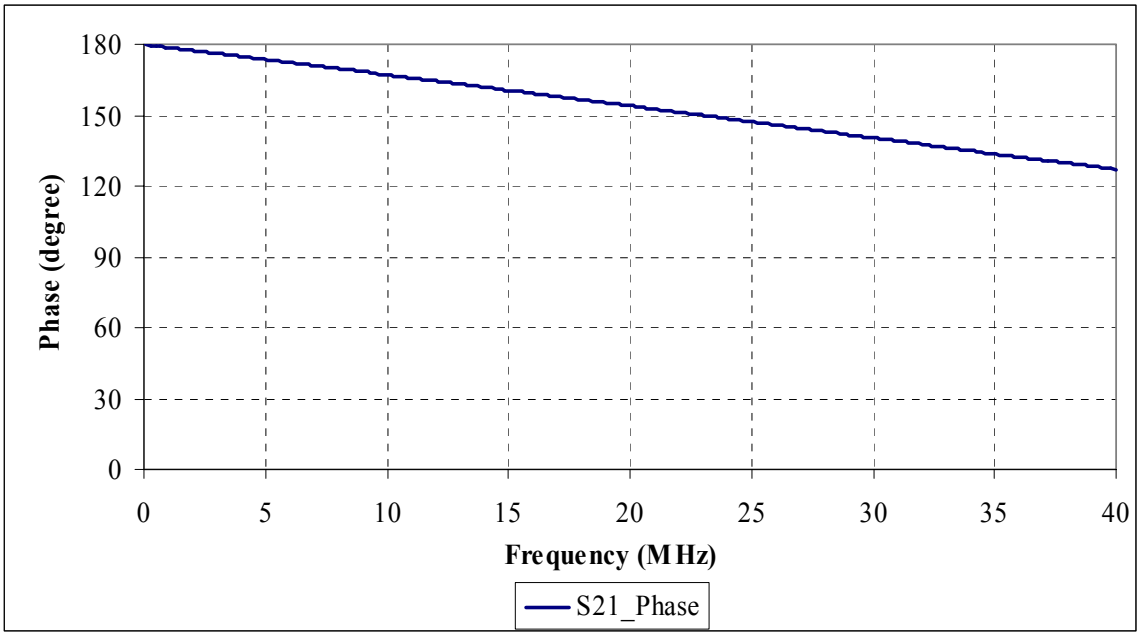

Figure 4.13: The transfer function (S_{21}) of the preamplifier in terms of phase (in degrees).

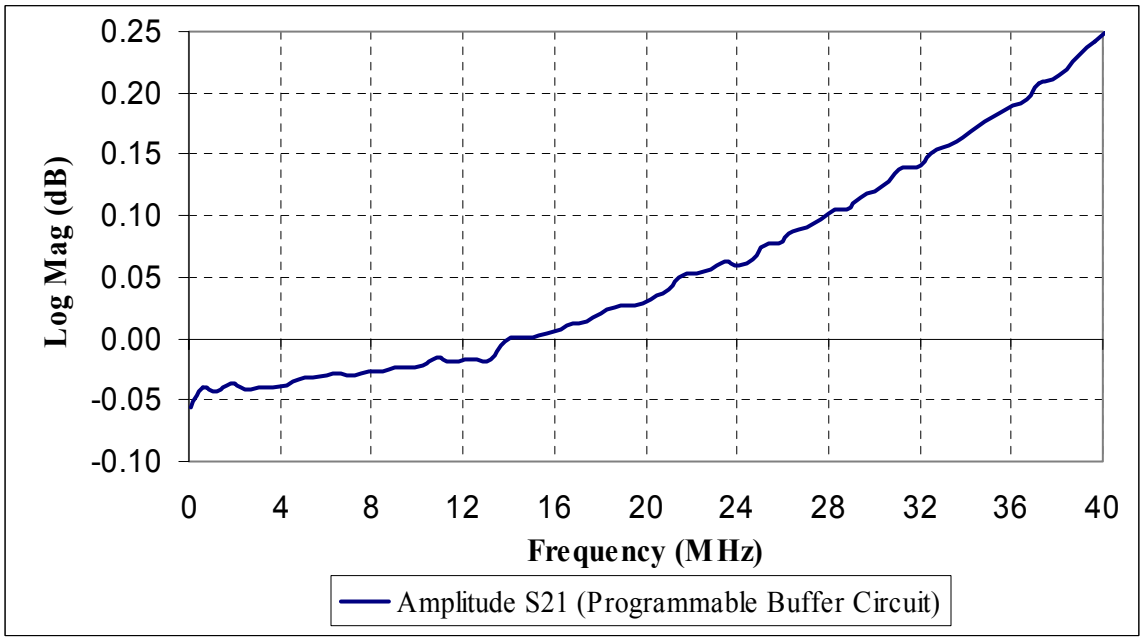

Figure 4.14: The transfer function (S_{21}) of the programmable buffer circuit in terms of magnitude (in dB).

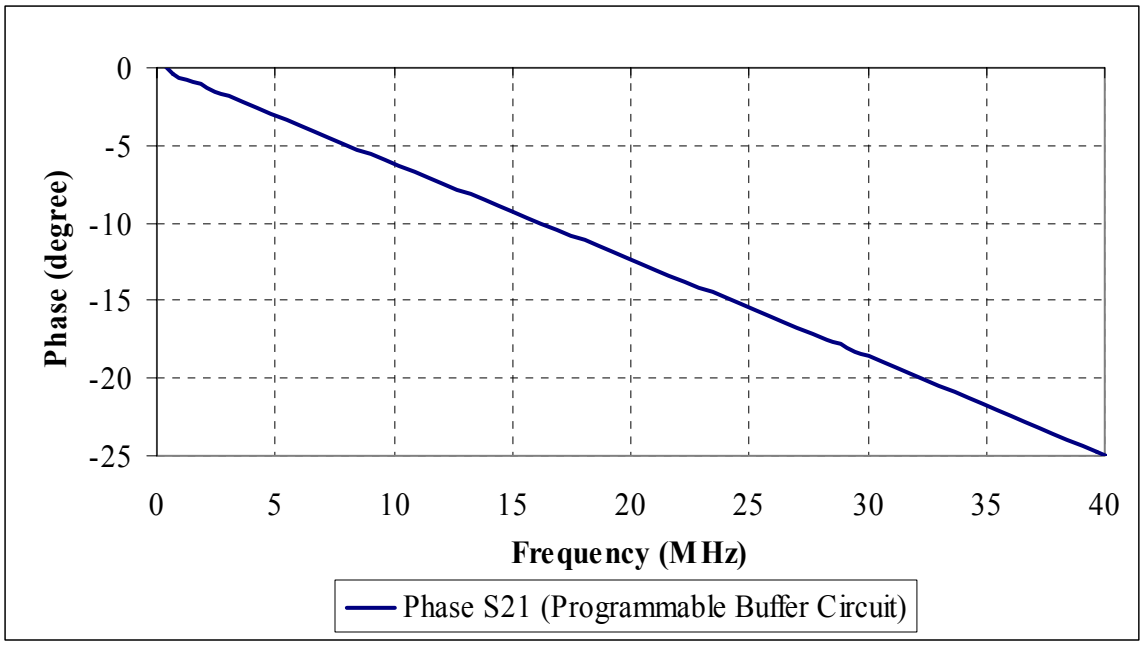

Figure 4.15: The transfer function (S_{21}) of the programmable buffer circuit in terms of phase (in degrees).

4.3.3 Acoustic Test

This section presents the results of the acoustic test performed during actual calibration of hydrophones using Time Delay Spectrometry (TDS) method, detailed in [37]. For this work, one needle-type hydrophone (NTR889) and one membrane-type hydrophone (804-022) were calibrated in the frequency range 0.1 to 40 MHz. The results of these measurements were analyzed to determine the performance of the programmable preamplifier assembly. The calibration results were obtained using a 0.5 mm diameter active area bilaminar membrane hydrophone (IP26). This hydrophone was previously calibrated and was considered the working reference hydrophone in this work. Figure 4.16 contains the frequency response of the NTR 889 needle-type hydrophone with and without the programmable preamplifier, shown for comparison. Also, the result of the

calibration with and without the programmable preamplifier for the 804-022 membrane-type hydrophone is shown in Figure 4.17.

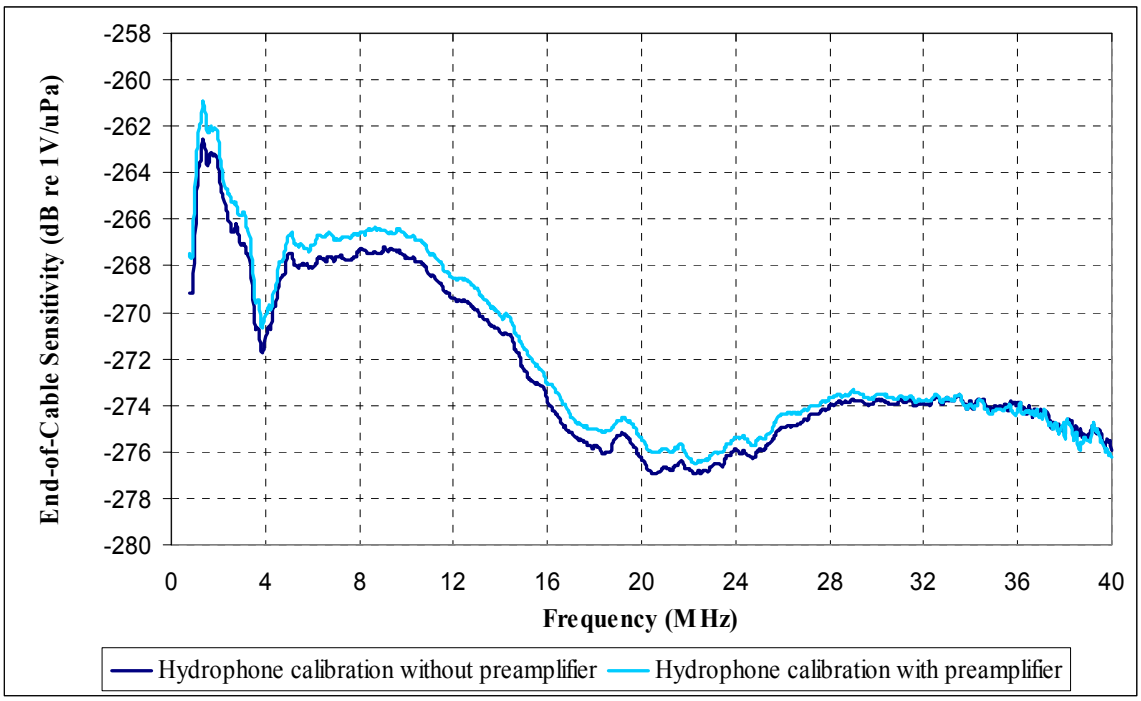

Figure 4.16: NTR 889 Needle-Type Hydrophone Calibration with/without the prototype programmable preamplifier.

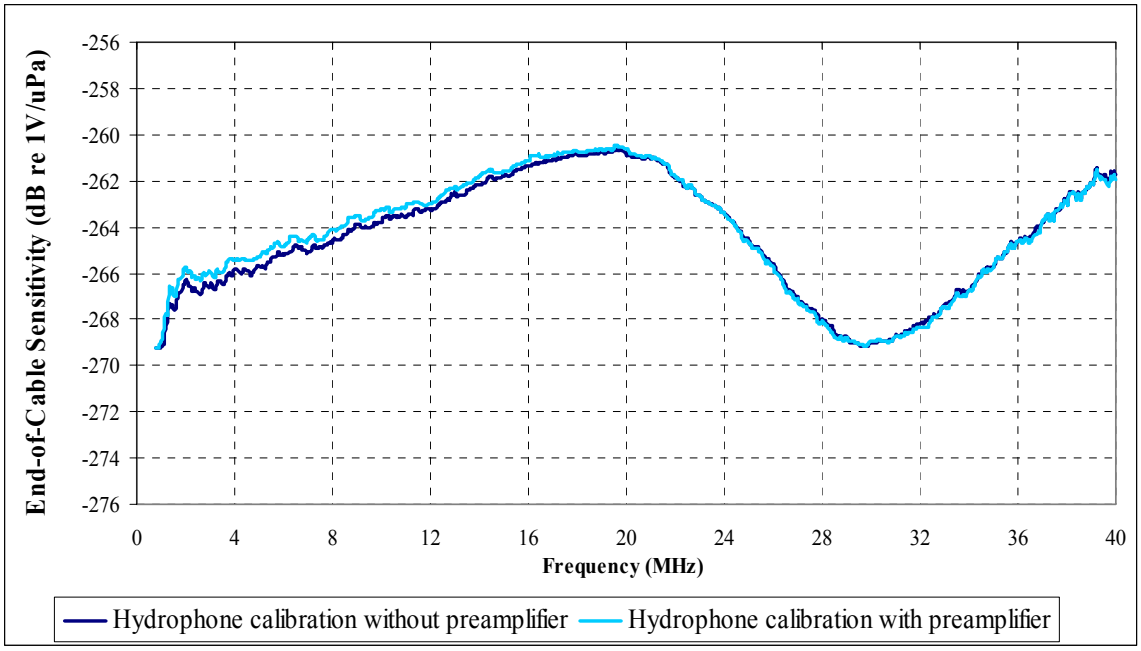

Figure 4.17: 804-022 Membrane-Type Hydrophone Calibration with/without the prototype programmable preamplifier.

CHAPTER 5.0: DISCUSSION AND CONCLUSIONS

The programmable preamplifier was simulated by the Pspice program and then tested using both electronic and acoustic methods in the frequency range between 100 kHz and 40 MHz. The results presented in the previous section show that the agreement between the simulations and experiments was very good.

Three different sets of feedback resistors (R_1, R_2, R_3, R_4, R_5, R_6 and R_7) in the preamplifier circuit topology in Figure 3.2 were simulated in order to show the optimum values as presented in Figure 4.1 and 4.2. The result of the magnitude transfer function as shown in Figure 4.1 of R_f 1 kOhms set was around 1 dB gain, whereas that of R_f 402 Ohms was approximately 0.03 dB gain and that of 200 Ohms was 0.08 dB. Therefore, the transfer function of R_f 402 Ohms set was found to be closet to the 0 dB gain and considered as the optimum set of resistors.

Figure 4.3 shows the transfer function (magnitude) simulation of the preamplifier from Pspice program in the frequency range between 100 kHz and 40 MHz. The result exhibited a uniform response (less than 0.035 dB) over the entire range of frequencies. Figure 4.4 presents the simulation of its phase. The phase of the preamplifier is found to be approximately 180 degrees at the low frequency and decreases as the frequency increases. The transfer function simulation of the programmable buffer circuit is presented in Figure 4.5. Also, the result was found to be consistent (to within ±0.3 dB) in the frequency range between 100 kHz and 40 MHz. Its phase, shown in Figure 4.6, was

found to be around 0 degrees at the low frequency and decreased when the frequency was increased. These simulation tests verified the agreement between the simulations and the design's objectives that the preamplifier and programmable buffer circuit have an over all gain of one or equal to 0 dB over the entire frequency range between 100 kHz and 40 MHz.

The magnitude and phase of impedance, Z, of the prototyping preamplifier, needle-type hydrophone and membrane-type hydrophone were measured using a network analyzer in the frequency range of 100 kHz to 40 MHz at 200 kHz intervals as shown in Figure 4.8 and 4.9. In Figure 4.8, the magnitude Z of all testing devices decreases when the frequency increases. However, the magnitude Z of the constructed preamplifier is even higher (more than 10 times) than the magnitude Z of the needle-type and membrane-type hydrophone. On the other hand, the phase Z values of the needle-type, membrane-type hydrophone and prototyping preamplifier increase with increasing frequency as shown in Figure 4.9. However, the phase Z values of the prototyping preamplifier are still lower than the phase Z values of the needle-type and especially the membrane-type hydrophone. These results verified that the tested preamplifier prototype has sufficiently high input impedance and does not load the output of the hydrophone, which can influence the voltage sensitivity vs. frequency characteristics of the hydrophone. From Figure 4.9, the membrane-type hydrophone data seem to indicate that the measurements at high frequencies are being dominated by an inductive contribution because its phase changes sign at the high frequencies. Therefore, the admittance measurement was carried

out to determine this result as shown in Figure 4.10 and 4.11. The results in Figure 4.10 and 4.11 implied the equivalent circuit as shown in Figure 5.1.

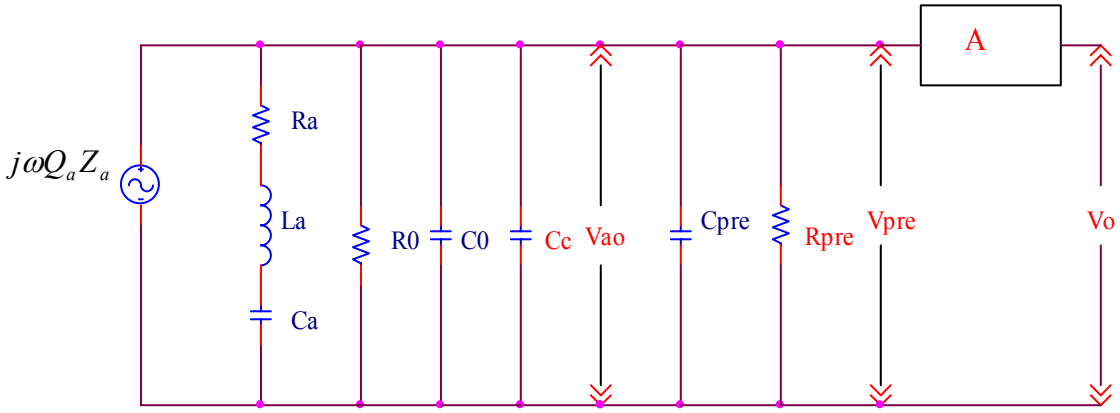

Figure 5.1: Equivalent circuit of preamplifier with the membrane-type hydrophone.

From Figure 5.1, it can be seen that the charge Q_a produced by a hydrophone when exposed to acoustic pressure appears as a voltage V_a. This voltage is developed across the motional impedance Z_a, clamped dielectric capacitance C_0, and dielectric losses R_0 of the hydrophone. However, the voltage V_{ao} appears when the hydrophone is loaded by the impedance, Z_{ao}, which includes the hydrophone impedances and the parallel capacitance (C_c) of the output connection cable. Therefore;

$$V_{ao} = j\omega Z_{ao} Q_a \tag{5.1}$$

where;

$$Y_{ao} = j\omega(C_0 + C_c) + \frac{1}{R_0} + \frac{1}{R_a + \frac{1}{j\omega C_a} + j\omega L_a} \tag{5.2}$$

or;

$$Z_{ao} = \frac{1}{j\omega C_c + j\omega C_0(1 + \frac{1}{j\omega C_0 R_0} + \frac{C_a}{C_0(1 - \omega^2 L_a C_a + j\omega C_a R_a)})} \tag{5.3}$$

From the equation 5.3, the term $\frac{1}{j\omega C_0 R_0}$ is the electrical loss tangent and $\frac{1}{j\omega C_a R_a}$ is the mechanical loss tangent of the PVDF, which are relatively small at low frequencies; however, at high frequencies their contributions are non-negligible. Also, the dramatic change of the membrane-type hydrophone's phase at the high frequencies in Figure 4.11 exhibited that the resonance frequency of the membrane-type hydrophone is ~37 MHz. This corresponds to the thickness resonance of the (double 15 μm layer) $30\,\mu m$ piezoelectric film when the thickness resonance is related to the 1/2 wavelength thickness of the piezoelectric polymer with sound velocity of 2.2 km/s.

The Scattering parameter S_{21} measurement was used to measure the transfer function (in dB) characteristics of the prototyping preamplifier and programmable buffer circuit in the frequency range of 100 kHz to 40 MHz at 200kHz intervals. The magnitude of the transfer function (S_{21}) response for the prototyping preamplifier, shown in Figure 4.12, exhibited a uniform response (± 0.3 dB) over the entire frequency range and its phase, shown in Figure 4.13, was found to be approximately 180 degree shift at the low

frequency and decreased when the frequency increased. Also, Figure 4.14 shows the magnitude of transfer function (S_{21}) response for the prototyping programmable buffer circuit that featured a very flat frequency response, to within ± 0.25 dB, in the frequency range 100 kHz – 40 MHz. The phase of prototyping programmable buffer circuit was around 0 degree shift at the low frequency and decreased with increasing frequency as shown in Figure 4.15. These results verified the unity gain objective of both the prototyping preamplifier and programmable buffer circuit.

The frequency response of the needle-type hydrophone with the preamplifier, shown in Figure 4.16, shows the sensitivity response somewhat higher (nearly 1 dB) in the frequency range from 2 MHz to 26 MHz than the frequency response without the preamplifier. In comparison to the membrane-type hydrophone, which has a uniform frequency response (± 4 dB), the needle-type exhibits response that is not really uniform (± 7 dB). Also, the frequency response of the membrane-type hydrophone with the preamplifier had somewhat higher sensitivity, which is around 0.5 dB in the frequency range between 2 MHz to 16 MHz, compared to that without preamplifier as shown in Figure 4.17. This could be caused by loading effect of the hydrophone's output without preamplifier that reduces the sensitivity. Also there is a significant finite amplitude distortion in the pressure wave especially at the low frequency, as mentioned in [2, 3].

In conclusion, the preamplifier and the programmable buffer circuit are useful devices in acoustic measurement chain. The prototyping preamplifier can perform an excellent impedance matching between the output impedance of the hydrophone and the input

impedance of the measuring instrument used to display or record the acoustic pressure-time waveforms. It also increases the overall hydrophone's sensitivity, which is beneficial in cases where the measured pressure amplitude is relatively low or when a significant finite amplitude distortion in the pressure wave is present [2, 3]. Moreover, the preamplifier prototype tested can eliminate the reflection effect from the transmission line phenomena.

Visual Basic program was successfully employed to automatically execute On/Off function of the programmable buffer circuit. With the application of the programmable buffer circuit, whenever the calibration process is done, the signals exciting the acoustic source is automatically cut off. Therefore, the acoustic source, such as a very wideband transducer, is not overexposed for a prolonged period of time.

When the programmable buffer circuit and the preamplifier are combined together and controlled via LabVIEW programs, the implemented circuit topology allows fully automatic determination of key acoustic output parameters of diagnostic ultrasound scanners, which determine the safety indicators such as Mechanical Index (MI) and Thermal Index (TI).

CHAPTER 6.0: FUTURE WORK

Although the programmable preamplifier has been included in the acoustics measurements, improvements to the overall system could be made to enhance the measurement system's performance. As already mentioned, the current programmable preamplifier could be used to operate in the frequency range between 100 kHz and 40 MHz. However, many new clinical applications of ultrasound imaging will operate at frequencies greater than 40 MHz. Therefore, the frequency range of the preamplifier and programmable buffer assembly should be extended to 100 MHz.

In terms of dynamic range, the existing programmable preamplifier was designed and could have been used to operate with a gain of one or 0 dB; however, in some applications the output signal from the hydrophone was relatively weak. Therefore, it is desirable to include 20 dB or 10x gain in the next improved prototype of the programmable preamplifier system. The programmable buffer circuit with adjustable gains, placed at position in Figure 6.1, would also offer a possibility to optimize dynamic range.

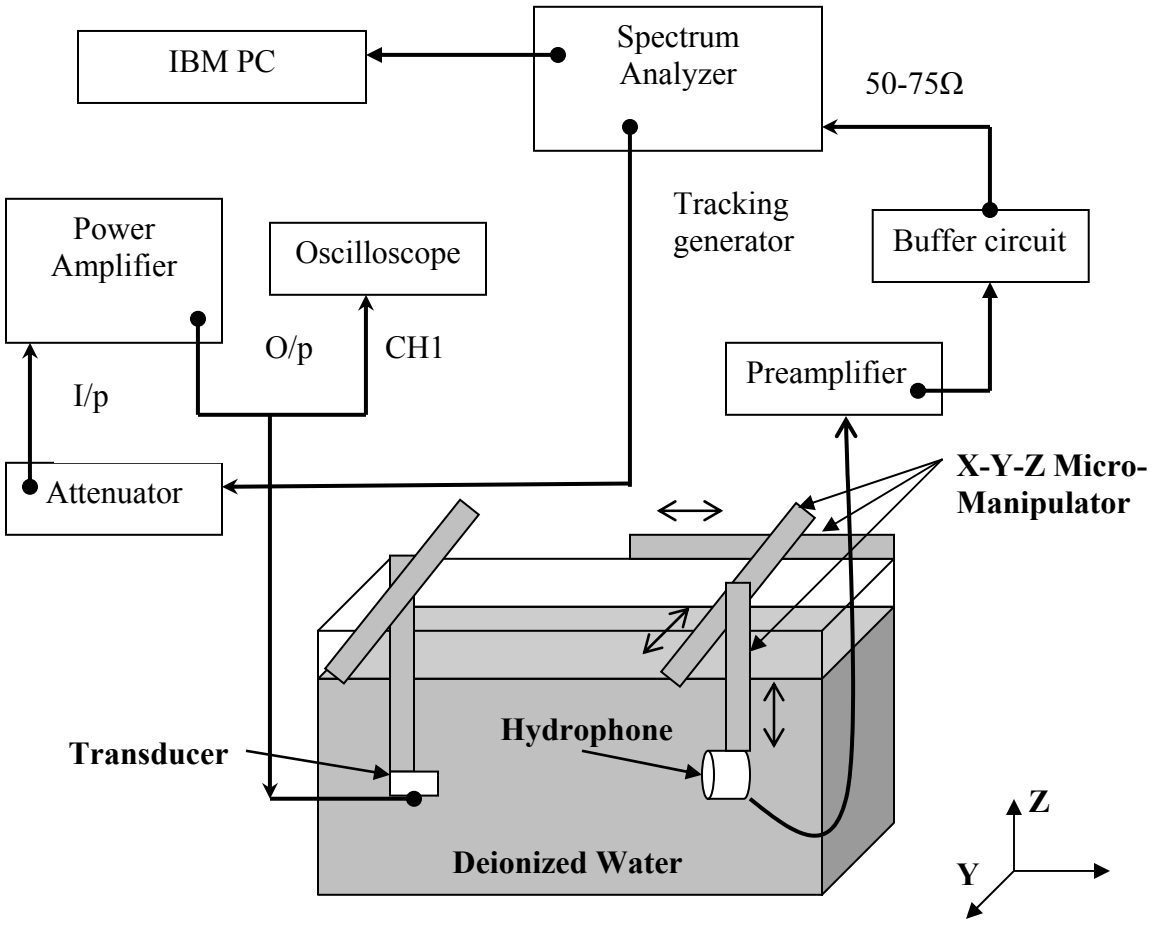

Figure 6.1: The measurement arrangement for an acoustics test with an adjustable programmable buffer circuit.

LIST OF REFERENCES

[1] C. Patton, G. R. Harris, R. A. Philips, "Output levels and bioeffects indices from diagnostic ultrasound exposure data reports o the FDA," *IEEE Trans. Ultrason. Ferroelec. Freq. Contr.*, vol. 41 no. 3, pp. 353-59, 1994

[2] G. R. Harris, "Hydrophone measurements in diagnostic ultrasound fields," *IEEE Trans. Ultrason. Ferroelec. Freq. Contr.*, vol. 35 no. 2, pp. 87-101, 1988

[3] R. A. Smith, "The importance of the frequency response of a hydrophone when characterizing medical ultrasonic fields," *Proc. Inst. Acoustics*, vol. 8 part 2, pp. 119-28, 1986

[4] P. A. Lewin, M. E. Schafer, R. C. Chivers, "Integrated Preamplifiers for Ultrasound Transducers," *Ultrasonics Symposium*, 0090-9607/85/0000-0503, pp. 503-506, 1985

[5] R. C. Preston, A. J. Livett, D. R. Bacon, "Absolute calibration of the hydrophones in the frequency range 0.5 MHz to 15 MHz," *Proc. Inst. Acoustics*, vol. 6 pt. 5, pp. 60-67, 1984

[6] M. Berson, J. M. Grégoire, F. Gens, J. Rateau, F. Jamet, L. Vaillant, F. Tranquart, L. Pourcelot, "High frequency (20 MHz) ultrasonic devices: advantages and applications," *European Journal of Ultrasound*, vol. 10 no.1, pp. 53-63, 1999

[7] H. Alexander, D. L. Miller, "Determining skin thickness with pulsed ultrasound," *J. Invest. Dermatol*, vol. 72 no. 1, pp. 17-19, 1979

[8] J. Serup, "Non invasive quantification of psoriasis plaques. Measurement of skin thickness with 15 MHz pulsed ultrasound," *Clin. Exp. Dermatol,* vol. 9 no. 5, pp. 502-508, 1984

[9] P. A. Payne, "Application of ultrasound in dermatology," *Bioeng. Skin***,** vol. 1 no. 4, pp. 293-320, 1985

[10] P. A. Payne, "Ultrasonic methods for skin characterization," *Bioeng. Skin,* vol. 3 no. 4, pp. 347-357, 1987

[11] M. D. Sherar, B. G. Starkoski, F. S. Foster, "A 100 MHz B-scan ultrasound backscatter microscope," *Ultrason. Imaging*, vol. 11 no. 2, pp. 95-105, 1989

[12] G. R. Lockwood, J. W. Hunt, F. S. Foster, "Design of protection circuitry for high frequency ultrasound systems," *IEEE Trans. Ultrason. Ferroelec. Freq. Contr*, vol. 38 no. 1, pp. 48-55, 1991

[13] C. J. Pavlin, K. A. Harasiewicz, F. S. Foster, "Ultrasound biomicroscopy of anterior structures in normal glaucomatous eyes," *Am. J. Ophtalmol*, vol. 113 no. 4, pp. 381-389, 1992

[14] D. H. Turnbull, B. G. Starkoski, K. A. Harasiewicz, et al., "A 40-100 MHz B-scan ultrasound backscatter microscope for skin imaging," *Ultrasound Med. Biol.*, vol. 21 no. 1, pp. 79-88, 1995

[15] H. S. Frew, R. A. Giblin, "The choice of ultrasound frequency for skin blood flow investigation," *Bioeng. Skin*, vol. 1 no. 3, pp. 193-205, 1985

[16] M. Berson, F. Patat, Z. Q. Wang, D. Besse, L. Pourcelot, "Very high frequency pulsed Doppler apparatus," *Ultrasound Med. Biol*, vol. 15, pp. 121-132, 1989

[17] D. A. Christopher, P. N. Burns, J. Armstrong, F. S. Foster, "A high frequency continuous-wave Doppler ultrasound system for the detection of blood flow in the microcirculation," *Ultrasound Med. Biol*, vol. 22 no. 9, pp. 1191-1203, 1996

[18] D. A. Christopher, P. N. Burns, B. G. Starkoski, F. S. Foster, "A high frequency pulsed-wave Doppler ultrasound system for the detection and imaging of blood flow in the microcirculation," *Ultrasound Med. Biol*, vol. 23 no. 7, pp. 997-1015, 1997

[19] "Standard for Real-time Display of Thermal and Mechanical Acoustic Output Indices on Diagnostic Ultrasound Equipment." Acoustical Institute of Ultrasound in Medicine, Laurel, MD, 1998

[20] "Acoustic Output Measurement Standard for Diagnostic Ultrasound Equipment." Acoustical Institute of Ultrasound in Medicine, Laurel, MD, 1998

[21] P. A. Lewin, G. Lypacewicz, R. Bautista, V. Devaraju, "Sensitivity of ultrasonic hydrophone probes below 1 MHz," *Ultrasonics*, vol. 38 no. 1-8, pp. 135-139, 2000

[22] J. M. Fiore, Op Amps & Linear Integrated Circuits, Delmar Thomson Learning, Albany, New York, 2001

[23] A. S. Sedra, K. C. Smith, Microelectronic Circuits, Oxford University Press 3rd Edition, New York, New York, 1991

[24] H. Johnson, "Scattering Parameters," High-speed digital design, vol. 6 no. 3 http://www.sigcon.com/

[25] M. C. Ziskin, P. A. Lewin (eds), Ultrasonic Exposimetry, CRC Press, Boca Raton, Florida, 1993

[26] P. A. Lewin, "Miniature piezoelectric polymer ultrasonic hydrophone probes," Ultrasonics, vol. 19, pp. 213-16, 1981

[27] G. R. Harris, "Sensitivity considerations for PVDF hydrophones using the spot-poles membrane design," *IEEE Trans. Ultrason. Ferroelec. Freq. Contr.*, vol. SU-29 no. 6, pp. 370-77, 1982

[28] D. R. Bacon, "Characteristics of a PVDF membrane hydrophone for use in the range 1-100 MHz," *IEEE Trans. Son. and Ultrason.*, vol. SU-29 no. 1, pp. 18-25, 1982

[29] P. A. Lewin, "Miniature piezoelectric polymer hydrophones in biomedical ultrasonics," *Ferroelectrics*, vol. 60, pp. 127-39, 1984

[30] P. Lum, M. Greenstein, C. Crossman, T. L. Szabo, "High-frequency membrane hydrophone," *IEEE Trans. Ultrason. Ferroelec. Freq. Contr.*, vol. 43 np. 4, pp. 536-43, 1996

[31] S. W. Meeks, K. Y. Ting, "Effects of static & dynamic stress on piezoelectric and dielectric properties of PVF2," *Acoustical society of America Journal*, vol. 74 (6), pp. 1681-1686, 1984

[32] R. A. Smith, "The importance of the frequency response of a hydrophone when characterizing medical ultrasonic fields" *Proc. Inst. Acoustics*, vol. 8 part 2, pp. 119-28, 1986

[33] G. R. Harris, "A model of the effects of the hydrophone and amplifier frequency response on ultrasound exposure measurements," *IEEE Trans. Ultrason. Ferroelec. Freq. Contr.*, vol. 38 no. 5, pp. 413-17, 1991

[34] D. G. Shombert, G. R. Harris. "Use of miniature hydrophones to determine peak intensities typical of medical ultrasound devices," *IEEE Trans. Ultrason. Ferroelec. Freq. Contr.*, vol. 33 no. 3, pp. 287-93, 1986

[35] G. Ludwig, K. Brendel, "Calibration of hydrophones based on reciprocity and Time Delay Spectrometry," *IEEE Trans. Ultrason. Ferroelec. Freq. Contr.*, vol. 35 no. 2, pp. 168-74, 1988

[36] P. Pederson, P. A. Lewin, L.Bjorno, "Application of Time Delay Spectrometry for calibration of ultrasonic transducers," *IEEE Trans. Ultrason. Ferroelec. Freq. Contr*., vol. 35 no. 2, pp. 185-205, 1988

[37] P. A. Lewin, "Calibration and performance evaluation of miniature ultrasonic hydrophones using Time Delay Spectrometry," Proc. *IEEE Ultrasonics Symposium*, pp. 660-64, 1981

APPENDIX A: LIST OF SYMBOLS

λ	Wavelength
C	Capacitance
CMR	Common Mode Rejection
C_a	Internal capacitance of the hydrophone
C_c	Parallel capacitance of hydrophone's output connection cable
C_p	Parallel capacitance
C_{pre}	Input capacitance of the preamplifier
DUT	Device under Test
f_{SR}	Frequency at which an output sinusoid with amplitude equal to the rated output voltage of the OP-AMP begins to show distortion due to slew-rate limiting
IA	Instrumentation Amplifiers
Im(Z)	Imaginary portions of the hydrophone's complex impedance
$Im(Z_{el})$	Imaginary components of the complex impedance of the measuring device
L_a	Internal inductance of the hydrophone
M	Sensitivity of the hydrophone being calibrated
MI	Mechanical Index
M_{ref}	Sensitivity of the reference hydrophone
$M_c(f)$	End-of-cable open-circuit sensitivity

$M_L(f)$	End-of-cable loaded sensitivity of a hydrophone
NA	Network Analyzer
OP-AMPs	Operational Amplifiers
p	Free-field acoustic pressure at the hydrophone
Q_a	Charge produced by a hydrophone when received acoustic pressure
R	Resistance
R_a	Internal resistance of the hydrophone
R_f	Feedback resistor
R_i	Input resistor
R_p	Parallel resistance
R_{pre}	Input resistance of the preamplifier
Re(Z)	Real portions of the hydrophone's complex impedance
$Re(Z_{el})$	Real components of the complex impedance of the measuring device
SA	Spectrum Analyzer
S_{21}	Scattering parameters (transfer function)
S_q	Hydrophone's charge sensitivity
S_v	Hydrophone's voltage sensitivity
TDS	Time Delay Spectrometry
TI	Thermal Index
U	Terminal voltages of the uncalibrated hydrophone
U_{ref}	Terminal voltages of the standard hydrophone
V	Rated voltage

v	Voltage generated by the acoustic pressure incident on the sensitive element of the hydrophone
V_a	Voltage produced by a hydrophone when exposed to acoustic pressure
V_{ao}	Voltage appears at the impedance which includes the hydrophone impedances and the parallel capacitance (C_c) of the output connection cable
V_i	Input Voltage
V_o	Output Voltage
Z_a	Internal impedance of the hydrophone
Z_{ao}	Impedance includes the hydrophone impedances and the parallel capacitance (C_c) of the output connection cable
Z_{pre}	Input impedance of the preamplifier

APPENDIX B: VISUAL BASIC PROGRAM

Visual Basic programming is employed to automatically execute On/Off function of the programmable buffer circuit. The program sends an ASCII character code 0 for Off stage and code 3 for On stage. These data are transferred via the RS232 serial port to Bitabug2 controller. The Visual Basic source code is shown in the Table B1. This program responds to data at 9600 baud rates on COM2 Port. Default parameters are used for the serial port setup. This includes 8 data bits, 1 stop bit, and no parity.

Table B1: The Visual Basic source code

```
Private Sub Command1_Click(Index As Integer)
   If Command1(Index).Caption = "OFF" Then
         Command1(Index).Caption = "ON"
   Else
         Command1(Index).Caption = "OFF"
   End If

   dat = 0
   If Command1(0).Caption = "ON" Then dat = dat + 3

   MSComm1.Output = Chr$(dat)

End Sub
```

```
Private Sub Form_Load( )
  MSComm1.Settings = "9600, n, 8, 1"      'Set Baud Rate
  MSComm1.CommPort = 2                    'Set the Comm Port
  MSComm1.PortOpen = True                 'Open the Comm Port
  Form1.Visible = True                    'Show the Interface

End Sub
```

Programming Result

Figure B1 presents the result after running the Visual Basic source code in the Table B1. In order to switch from On to Off or from Off to On function, just click on the buffer output button.

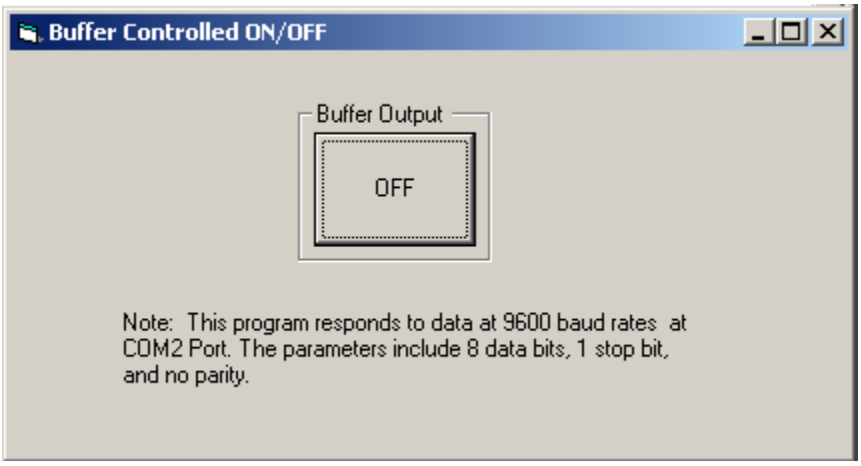

Figure B1: The result screen of the Visual Basic after running the source code in the Table B1.

APPENDIX C: BOARD LAYOUT GUIDELINES

C.1 Minimize the distance

The distance from the power supply pins to 0.1μF decoupling capacitor for the OPA643 and to 10μF bypass capacitor for the OPA355 should be less than 0.25 inches to avoid narrow power and ground traces, which minimize inductance between pins and the capacitors.

C.2 Careful selection and placement of external components

Careful selection and placement of external components will preserve the high frequency performance of the preamplifier and programmable buffer circuit. Metal film and carbon composition resistors are used in the prototypes. These types of resistors can provide good high frequency performance. Never use wirewound type resistors in a high frequency application. However, keep their leads and PC board trace length as short as possible since the output pin and inverting input pin are the most sensitive to parasitic capacitance; always position the feedback and series output resistor as close as possible to the output pin. Other network components, such as non-inverting input termination resistors, should also be placed close to the OP-AMP package. In the prototypes, double side component mounting is used and the feedback resistor are placed directly under the

OP-AMP package on the other side of the board between the output and inverting input pins in order to minimize parasitic capacitance.

C.3 No socketing in a high speed OP-AMPs

Several experiments indicated that socketing of both OPA643 and OPA355 OP-AMPs is not recommended. The additional lead length and pin-to-pin capacitance introduced by the socket can create an extremely troublesome parasitic network, which can make it almost impossible to achieve a smooth, stable frequency response. Best results were obtained by soldering the OPA643 and OPA355 onto the board directly.